© 2019. Published by The Company of Biologists Ltd | Development (2019) 146, dev177097. doi:10.1242/dev.177097

RESEARCH ARTICLE

Abiotic stress modulates root patterning via ABA-regulated microRNA expression in the endodermis initials

Daria Bloch[1], Malikarjuna Rao Puli[1], Assaf Mosquna[2] and Shaul Yalovsky[1,*]

ABSTRACT

Patterning of the root xylem into protoxylem (PX) and metaxylem is regulated by auxin-cytokinin signaling and microRNA *miR165a*/*166b*-mediated suppression of genes encoding Class III HOMEODOMAIN LEU-ZIPPER (HD-ZIPIII) proteins. We found that, in *Arabidopsis*, osmotic stress via core abscisic acid (ABA) signaling in meristematic endodermal cells induces differentiation of PX in radial and longitudinal axes in association with increased *VND7* expression. Similarly, in tomato, ABA enhanced PX differentiation longitudinally and radially, indicating an evolutionarily conserved mechanism. ABA increased expression of *miR165a*/*166b* and reduced expression of the *miR165a*/*166b* repressor ZWILLE (ZLL) (also known as ARGONAUTE10), resulting in reduced levels of all five HD-ZIPIII RNAs. ABA treatments failed to induce additional PX files in a *miR165a*/*166b*-resistant *PHB* mutant, *phb1-d*, and in *scr* and *shr* mutants, in which *miR165a*/*166b* expression is strongly reduced. Thus, ABA regulates xylem patterning and maturation via *miR165a*/*166b*-regulated expression of HD-ZIPIII mRNAs and associated VND7 levels. In lateral root initials, ABA induced an increase in *miR165a* levels in endodermal precursors and inhibited their reduction in the future quiescent center specifically at pre-emergence stage. Hence, ABA-induced inhibition of lateral root is associated with reduced HD-ZIPIII levels.

KEY WORDS: ABA, Xylem, Root, *Arabidopsis*, Patterning, MicroRNA

INTRODUCTION

Arabidopsis primary xylem is composed of two cell types, a peripheral protoxylem (PX) and central metaxylem (MX) (De Rybel et al., 2016). Specification of the xylem axis is regulated by auxin-cytokinin (CK) feedback loops. Auxin induces vascular specification through MONOPTEROS (MP) [also known as AUXIN RESPONSE FACTOR 5 (ARF5)] (Hardtke and Berleth, 1998). In PX provascular cells, MP induces expression of the CK signaling inhibitor ARABIDOPSIS HISTIDINE PHOSPHOTRANSFER PROTEIN 6 (AHP6) (Bishopp et al., 2011; Mahonen et al., 2006).

In parallel, the radial patterning of PX and MX is regulated by the GRAS transcription factors SHORTROOT (SHR) and SCARECRAW (SCR), which, in the endodermis initials, induce the expression of two microRNAs (miRNAs) *miR165a* and *miR116b*. *miR165a* and *miR166b* move into the stele, presumably forming a local gradient, and restrict the expression of the Class III HOMEODOMAIN LEU-ZIPPER (HD-ZIPIII) family transcription factors PHABULOSA (PHB), REVOLUTA (REV), PHAVOLUTA (PHV), ATHB8 and ATHB15 [also known as CORONA (CNA)] to MX provascular cells. The low and high expression levels of HD-ZIPIII proteins in PX and MX provascular cells, respectively, are required for PX and MX specification (Carlsbecker et al., 2010; Miyashima et al., 2011).

The expression of HD-ZIPIIIs depends on local auxin biosynthesis in the root and its concentration by polar auxin transport (Bishopp et al., 2011; Muraro et al., 2014; Ursache et al., 2014). PHB induces local CK biosynthesis by inducing the expression of ISOPENTENYL TRANSFERASE 7 (IPT7) (Dello Ioio et al., 2012; Sebastian et al., 2015) and suppresses auxin signaling by induction of IAA20 and IAA30 auxin signaling inhibitors (Müller et al., 2016). Following specification in the meristem, the differentiation and maturation of PX and MX depend on the key transcriptional regulators VASCULAR DEPENDENT NAC DOMAIN 7 (VND7) and VND6, respectively (Kubo et al., 2005).

Abscisic acid (ABA) is a central regulator of abiotic stress responses in plants. ABA levels in roots increase rapidly in response to drought and salt stress (Audran et al., 1998; Geng et al., 2013; Qin and Zeevaart, 1999; Schachtman and Goodger, 2008). ABA signaling functions via intracellular receptors called PYRABACTIN RESISTANT1/PYR1 LIKE (REGULATORY COMPONENTS OF ABA RECEPTORS) [PYR1/PYL (RCAR)]. Upon binding ABA, PYR1/PYL sequester type 2C protein phosphatases (PP2C) leading to the activation of SUCROSE NON FERMENTING RELATED SERINE/THREONINE PROTEIN KINASE (SnRK) family kinases that phosphorylate ion channels and transcription factors (Fujii et al., 2009; Ma et al., 2009; Park et al., 2009; Parry et al., 2009). Different members of the PYR/PYL/RCAR family influence ABA signaling in the root (Antoni et al., 2013; Xing et al., 2016; Zhao et al., 2014). In addition, tissue-specific expression of the PP2C dominant mutant ABA INSENSITIVE 1 ($abi1^{G180D}$) inhibits ABA responses in roots (Duan et al., 2013; Geng et al., 2013).

In the primary root, ABA inhibits cell division of the quiescent center (Zhang et al., 2010). Inhibition of lateral root (LR) formation by ABA takes place at either the positioning/initiation or emergence stages (De Smet et al., 2003; Orman-Ligeza et al., 2018) at high or low ABA concentrations, respectively. Tissue specific expression of abi1-1 indicated that, at post-emergence, ABA-induced LR quiescence involves non-cell autonomous signaling from the primary root endodermis (Duan et al., 2013). *scr* and *shr* seedlings are ABA hypersensitive, and ABA response genes are direct targets of SCR (Iyer-Pascuzzi et al., 2011). In the stele, *VND7* cluster secondary wall-associated genes are upregulated in response to various stress stimuli, but although patterning regulators such as SCR are associated with stress responses, changes in radial patterning have not been observed upon stress (Iyer-Pascuzzi et al., 2011). Thus, the function of ABA in root patterning is not fully understood.

[1]School of Plant Sciences and Food Security, Tel Aviv University, Tel Aviv 6997801, Israel. [2]The Robert H. Smith Institute of Plant Sciences and Genetics in Agriculture, Faculty of Agriculture, The Hebrew University of Jerusalem, Rehovot 7610001, Israel.

*Author for correspondence (shauly@tauex.tau.ac.il)

M.R.P., 0000-0001-8271-8195; S.Y., 0000-0003-3264-0005

Received 19 February 2019; Accepted 23 July 2019

Development (2019) 146, dev177097. doi:10.1242/dev.177097

Our results demonstrate that osmotic stress and ABA influence xylem patterning by regulating levels of *miR165a/166b* and, as a result, HD-ZIPIII RNA and concomitantly *VND7* levels. Regardless of known negative effects of ABA on auxin responses, our analysis shows that the effects of ABA and auxin on xylem differentiation function via separate pathways. Moreover, our results show that ABA-induced LR quiescence at post-emergence stage is associated with an increase in *miR165a* and a reduction in PHB levels. During the preparation of this work, a complementary study demonstrating the effect of ABA on xylem patterning in the root was published (Ramachandran et al., 2018). This study demonstrated that osmotic stress via ABA regulates PX differentiation and MX continuity by affecting *miR165* expression.

RESULTS

ABA alters xylem patterning in the root in radial and longitudinal axes

Cell walls were stained with propidium iodide (PI), and the measurement of cortex cell lengths using the Cell-o-Tape ImageJ (Fiji) macro (French et al., 2012) allowed accurate identification of the end of the transition zone (ETZ) that outlines the termination of the root meristematic zone and the beginning of the rapid cell elongation/differentiation zone. The Cell-o-Tape analysis showed that following ABA treatments the ETZ was shorter, indicating that ABA induced earlier cell elongation and/or differentiation relative to the position of the quiescent center (QC) (Fig. S1). The accurate analysis of differentiation along the root longitudinal axis ensured that radial patterning was reproducibly analyzed at the same position.

The staining of root lignified secondary cell walls (SCW) with basic Fuchsin showed a significant increase after ABA treatments (Fig. S2A,B). Co-staining of roots with Calcofluor White, which labels cellulose, and basic Fuchsin enabled analysis of the position of xylem lignification relative to the ETZ, revealing the timing of differentiation. Lignified SCW in PX and MX appear at distance of 8 to 9 cells and 18 to 20 cells, respectively, indicating that their maturation is separated in time. Following ABA treatments, lignified SCW appeared in the PX at 5 to 6 cells away from the ETZ (Fig. 1A,B and Fig. S2C). Moreover, after ABA treatments additional files of PX appeared at the MX position at a distance of 8 to 9 cells from ETZ (Fig. 1A,C), indicating that ABA induces early differentiation of xylem.

In tomato (*Solanum lycopersicum*) variety M82, two PX files differentiate between 2.5-3 mm from the tip and an additional internal two PX files start to differentiate ∼5 mm from the tip (Fig. 1D-F and Fig. S3). Following treatment with 1 or 5 µM ABA, the external PX files start to differentiate 1.5 mm from the tip and the two internal files differentiate ∼2.2 mm from the tip (Fig. 1D-F and Fig. S3A-D). In addition, ABA causes differentiation of up to six PX files 5 mm from the tip (Fig. 1E and Fig. S3E,F). The identity of the PX cells in *Arabidopsis* was confirmed using the PX marker pS18:ER-GFP (Lee et al., 2006). Following ABA treatments, pS18:ER expression was also observed in the two MX provascular cell files adjacent to the PX, confirming their PX specification (Fig. 1G and Fig. S4A). Taken together, the analysis of *Arabidopsis* and tomato roots indicated that ABA primarily affects the timing of provascular cell differentiation. Next, we examined whether the early PX differentiation is associated with VND7.

We evaluated expression of *pVND7::GFP-NLS* (Kubo et al., 2005) after tissue clearing as previously described (Kurihara et al., 2015). *VND7* expression began in the cell division zone PX provascular cells located 3 to 4 cells distal to the QC. The expression levels were low and stable in the first 8 to 9 cells and then gradually increased (Fig. 1H,I and Fig. S4B,C). Following treatment with 5 µM ABA, expression of *VND7* in provascular PX appeared later (6 to 7 cells distal to the QC), but the expression levels increased significantly faster compared with control (Fig. 1H,I and Fig. S4C,D). Following ABA treatments, *pVND7::GFP-NLS* signal was also detected in MX provascular cells (Fig. 1H,J) and in the xylem pole pericycle cells in the elongation zone (Fig. S4B). The analysis of the *pVND7::GFP-NLS* signal distribution indicates that exogenous ABA treatment resulted in increased VND7 expression in the longitudinal and radial axes, which likely accounted for the earlier SCW formation.

Lignification of the Casparian strip (CS) in the endodermis is required for the formation of a functional diffusion barrier (Naseer et al., 2012). Fuchsin staining revealed that, in *Col-0* seedlings, lignification of the PX and CS in the endodermis were synchronized. CS lignification occurred around 9 to 10 cells from the ETZ. Following ABA treatments, CS lignification moved to 6 to 8 cells from ETZ (Fig. 1C,K). Collectively these results indicate that differentiation of PX and endodermis in roots is synchronized, and ABA induced earlier differentiation of these tissue layers.

Core ABA signaling and reduced water potential regulate xylem patterning

Next, the organization of vascular tissue in the maturation zone was examined in the region between 11 to 13 cells from ETZ. At this position, no MX differentiation occurs and two PX files are easily detected with PI staining (Fig. S1A). As mentioned above, ABA treatment induced the formation of additional PX cell files that were distinguished by their typical spiral cell wall pattern. Whereas wild-type (WT) plants constantly have two PX cell files, ABA treatments induced the appearance of one or two additional files, depending on ABA concentration. These extra PX files were on the inner side of the normal PX position and resulted from earlier differentiation of MX provascular cells (Fig. 2A,B and Fig. S5A).

Next, we asked whether the formation of the extra PX files depended on the core ABA signaling cascade. The roots of both the quadruple ABA receptor mutant (*pyr1;pyl1;pyl2;pyl4*) (Park et al., 2009) and *abi1-1*, which have a dominant mutation of PP2C phosphatase (Leung et al., 1994), had normal PX organization consisting of two files under control conditions. Following ABA treatments, however, fewer files of extra PX were formed (Fig. 2A,B and Fig. S5B,C). ABA signaling and responses can be induced in transgenic plants independently of exogenous ABA application by expressing an engineered PYR1 ABA receptor. In plants that express $PYR1^{Y58H/K59R/V81I/F108A/S122G/F159L}$ ($PYR1^{MANDI}$), mandipropamid triggers ABA responses (Park et al., 2015). Treatment of *35S::$PYR1^{MANDI}$* seedlings with mandipropamid induced a similar but stronger effect on root morphology than did ABA, resulting in earlier differentiation of root hairs and vascular tissues compared with control (Fig. S6A). Differentiation of MX provascular cells into PX occurred more efficiently following treatment with 5 µM mandipropamid than with ABA, and some *35S::$PYR1^{MANDI}$* roots treated with mandipropamid had five PX files (Fig. 2C and Fig. S6B). These results indicate that the core ABA signaling is required for ABA effects on the timing of PX differentiation and PX/MX specification.

As ABA mediates the responses to osmotic and salt stress, we asked whether either stress induces the formation of additional PX. No effect on PX differentiation was observed following incubation of roots for 24 h in 25, 50 or 100 mM NaCl (Fig. S7A). Similar to the effect of ABA, incubation in 60 g/l and 120 g/l polyethylene glycol 8000 (PEG 8000) for 24 h, which results in osmotic stress,

Development (2019) 146, dev177097. doi:10.1242/dev.177097

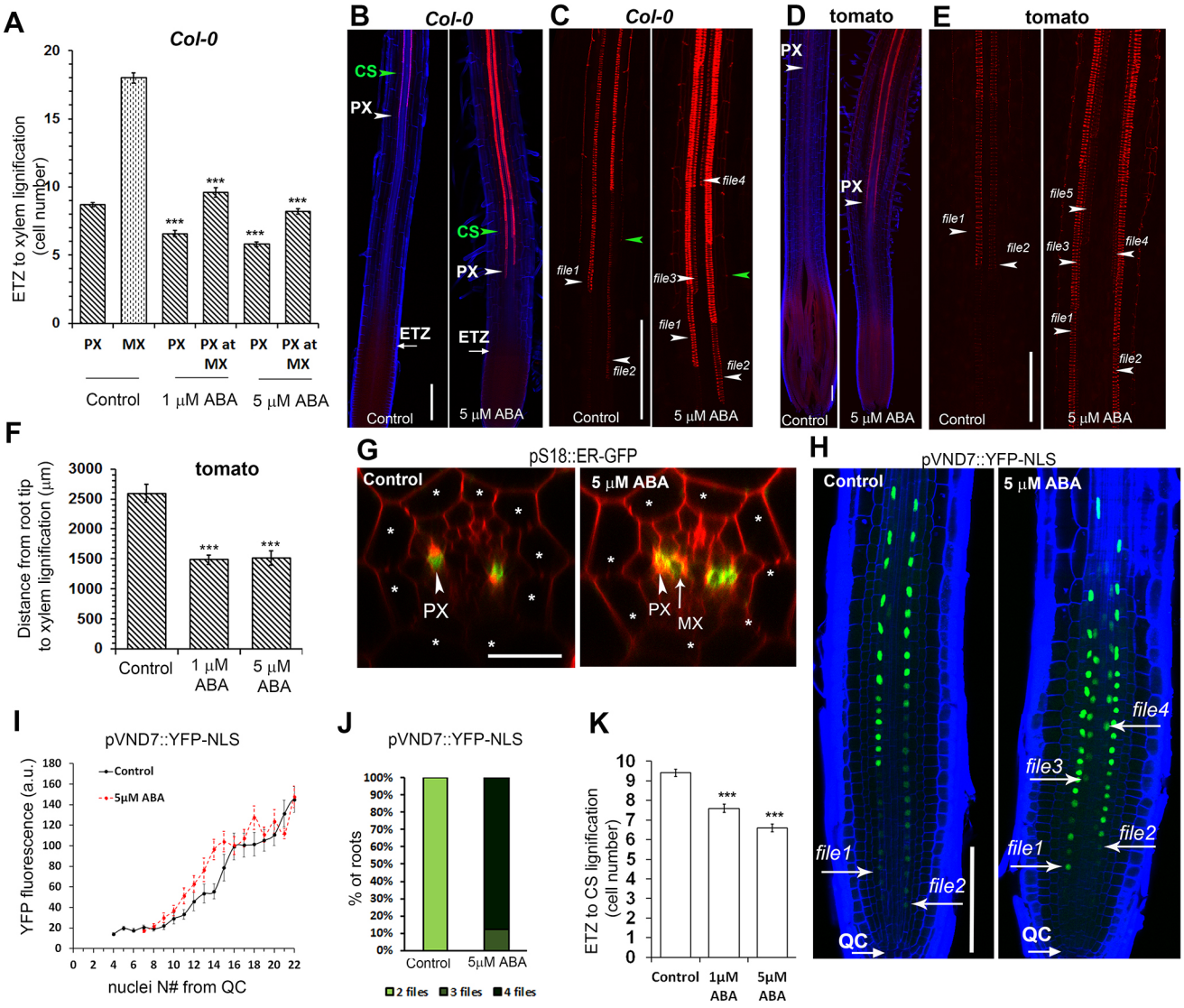

Fig. 1. Response of primary root to ABA. (A) Distance in cell number from ETZ to xylem lignification revealed by basic Fuchsin. For each treatment, distance was calculated for PX and MX position (control *n*=13; 1 µM ABA *n*=12; 5 µM ABA *n*=6). (B) Cleared *Col-0* roots stained with Calcofluor White (blue) and basic Fuchsin (red). Position of PX, Casparian strip (CS) and ETZ (arrows) are defined. (C) Close-up view of PX and CS in *Col-0* stained with basic Fuchsin. Lignified PX cell files are indicated with white arrowheads; green arrowheads mark CS. (D) Cleared *M82* tomato roots stained with Calcofluor White (blue) and basic Fuchsin (red). Position of PX is defined (white arrowheads). (E) Close-up view of PX in *M82* stained with basic Fuchsin. Lignified PX cell files are indicated with white arrowheads. (F) Distance from root tip to xylem lignification in *M82* revealed by basic Fuchsin (control *n*=4; 1 µM ABA *n*=6; 5 µM ABA *n*=6). (G) *z*-cross-sections of the PX marker *pS18::GFP-ER* (green; arrowheads). Note the appearance of the GFP signal at the MX position in ABA-treated roots (arrow). Cell walls were stained with PI (red). Asterisks mark the endodermis. (H) Expression of *pVND7::YFP-NLS* (green) in cleared roots. Cell walls stained with Calcofluor White (blue). Provascular PX cell files are indicated (arrows). QC→indicates quiescent center. (I) Mean YFP fluorescence intensity in nuclei of PX provascular cells (files 1 and 2 in H). Nuclei positions are relative to the QC (*n*=18 cell files per treatment). (J) Percentage of xylem *pVND7::YFP-NLS*-expressing cell files in control and roots treated with 5 µM ABA (*n*=15 roots per treatment). (K) Distance in cell number from ETZ to CS lignification (control *n*=12; 1 µM ABA *n*=12; 5 µM ABA *n*=6). Data are mean±s.e.m (A,F,K). ***$P \leq 0.0005$, Student's *t*-tests, two-tail distribution, unequal variance. Scale bars: 100 µm in B-E,H; 20 µm in G. See also Figs S1, S2, S3 and S4A-D.

induced the appearance of one or more additional files of PX in 80% of WT roots (Fig. 2D,E and Fig. S7B). PEG 8000 treatments also caused disordering of SCW in PX, leading to a variety of xylem patterns (Fig. S7C). To examine whether the influence of PEG 8000 on xylem differentiation was ABA-dependent, treatments were carried out using *pyr1;pyl1;pyl2;pyl4* and the *aba2-1* ABA biosynthesis mutant (González-Guzmán et al., 2002). Following incubation in 60 g/l PEG 8000, only one extra file of PX appeared in ∼20% of *pyr1;pyl1;pyl2;pyl4* and *aba2-1* roots (Fig. 2E and Fig. S7E). The reduced number of cells in xylem files in the ABA signaling and biosynthesis mutants suggests that PEG 8000 alters xylem differentiation in the root in a manner that depends on ABA biosynthesis and core ABA signaling. Incubation with 0.2 M sorbitol, which causes osmotic stress, similar to PEG8000, induced formation of additional xylem files in three out of nine seedlings (Fig. S7D).

ABA-regulated signaling PX specification takes place in meristematic endodermal precursors

To determine whether the meristem is required for ABA-induced PX differentiation, we excised the root tip at distances longer than 500 µm or shorter than 200 µm (Fig. 3A), which prevented or allowed, respectively, regeneration (Efroni et al., 2016; Sena et al.,

Development (2019) 146, dev177097. doi:10.1242/dev.177097

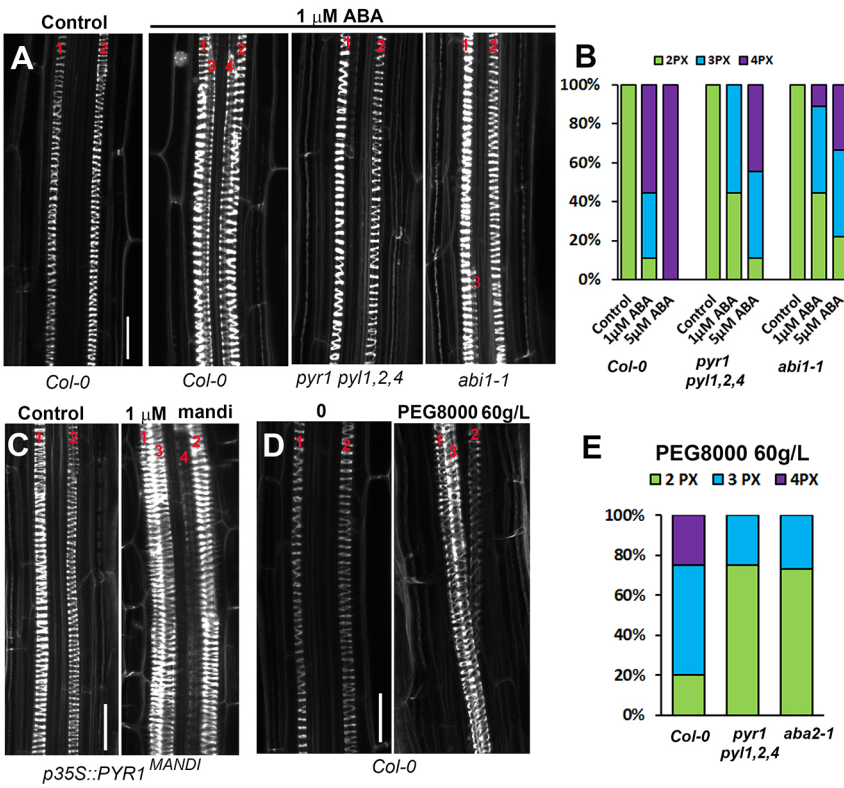

Fig. 2. ABA and osmotic stress induce formation of additional PX files. (A) Effect of 24 h treatment with 1 µM ABA on differentiation of PX in *Col-0*, *abi1-1* and *pyr1;pyl1;pyl2;pyl4* roots. Note that *abi1-1* and *pyr1;pyl1;pyl2;pyl4* mutants treated with 1 µM ABA developed three or two PX cell files, respectively (red digits). (B) Frequencies of PX cell file numbers after 24 h in control or ABA-treated conditions (n=9 for each genotype and treatment). (C) Xylem of *35S::PYR1*^{MANDI} following 24 h with 1 µM mandipropamid or control. (D) Col-*0* xylem following 24 h incubation in 60 g/L PEG8000. (E) Frequencies of PX files following PEG 8000 treatments of *Col-0* (n=20), *pyr1;pyl1;pyl2;pyl4* (n=20) and *aba2-1* (n=15) seedlings. All images are *z*-stack maximal projections of vascular tissues stained with PI (white) at distance of 11 to 13 cells from ETZ. Digits indicate PX cell files. Scale bars: 20 µm. See also Figs S5, S6 and S7.

2009). Excision of the root at distances longer than 500 µm from the tip prevented regeneration and abolished the ABA-induced PX differentiation from MX provascular cells. In contrast, when less than 200 µm was excised, the ABA treatment induced formation of ectopic PX (Fig. 3B and Fig. S8A). Excision at distances shorter than 200 µm, which removed the stem cell niche, likely allowed the respecification of cell identities required for the ABA-induced PX repatterning.

The lack of PX repatterning in ABA-treated roots that were excised at a distance longer than 500 µm from the tip suggests that cell respecification is crucial for the ABA effect. An alternative scenario that does not involve cell respecification is that there is a loss of a component or components required for maturation and radial patterning when the root is excised at distances longer than 200 µm from the tip. To distinguish between these scenarios, we examined whether cells that exit the meristematic zone respond to ABA. To this end, the position of the elongation zone initiation was labeled immediately before incubation in ABA (Fig. S8B, asterisk). With or without ABA treatment, the cells in the elongation zone did not form additional PX files, whereas MX was formed (Fig. 3C and Fig. S8C). This result indicates that ABA regulates PX/MX specification in the meristem and suggests that the effects of ABA on vascular patterning do not result from long-distance signaling between the meristem and the maturation zone.

Enhancer trap lines with tissue-specific expression of abi1-1 (Duan et al., 2013) were used to determine the tissue specificity of the ABA effect on PX differentiation. The ABA-induced differentiation of MX provascular cells into PX was repressed when abi1-1 was expressed in the endodermis in enhancer trap lines (Fig. 3D and Fig. S9: *J0571>>abi1-1* and *Q2500>>abi1-1*) and *pSCR* promoter driven abi1-1 lines (Fig. 3F,G). In comparison, expression of abi1-1 in the stele or in control lines harboring abi1-1 without a driver promoter did not repress the ABA-induced ectopic PX files differentiation (Fig. 3D,E and Fig. S9: *Q0990>>abi1-1*). Expression of abi1-1 in the columella also had mild inhibitory effects (Fig. 3D and Fig. S9: *J3411>>abi1-1*). Taken together, our results indicate that the ABA signaling that induces formation of additional PX cells takes place primarily in endodermal precursor cells in the meristem.

The mechanism of ABA-induced xylem maturation and repatterning

In the root meristem, auxin signaling upregulates the expression of the CK signaling inhibitor AHP6 to specify PX (Bishopp et al., 2011). AHP6 is expressed in the PX and adjacent pericycle cells (Mahonen et al., 2006). Imaging of cleared roots demonstrated that low levels of *pAHP6::GFP-ER* (*AHP6*) were also present in MX provascular cells with and without ABA treatment. Treatments with 1 µM ABA had no effect on the expression level or pattern of *AHP6*. Treatments with 5 µM ABA lowered the overall average *AHP6* expression but increased the variance and were not statistically significant (Fig. 4A,F and Fig. S10A). Given that ABA treatments did not result in increased *AHP6* expression in the MX provascular cells, it is unlikely that ABA affects xylem pattering via MP-mediated auxin signaling. To further explore the interaction between auxin and ABA in regulation of PX differentiation we examined the effect of ABA in seedlings treated with auxin signaling and transport inhibitors, and in auxin signaling mutants (Figs S11 and S12). Treatments with the auxin signaling inhibitor auxinole (Hayashi et al., 2008) strongly inhibited the auxin response (Fig. S11A-D) and the inhibition was slightly enhanced by co-treatments with ABA (Fig. S11C,D). These data agree with a known inhibitory effect of ABA on auxin responses (He et al., 2012; Shani et al., 2017). Treatments with auxinole completely abolished xylem formation, whereas treatments with 1-naphthylphthalamic acid (NPA) had no effect. Co-treatments with auxinole and ABA induced formation of a single file or two files of mature PX cells (Fig. S11E,F). Similar to auxinole, effects of ABA on xylem

Development (2019) 146, dev177097. doi:10.1242/dev.177097

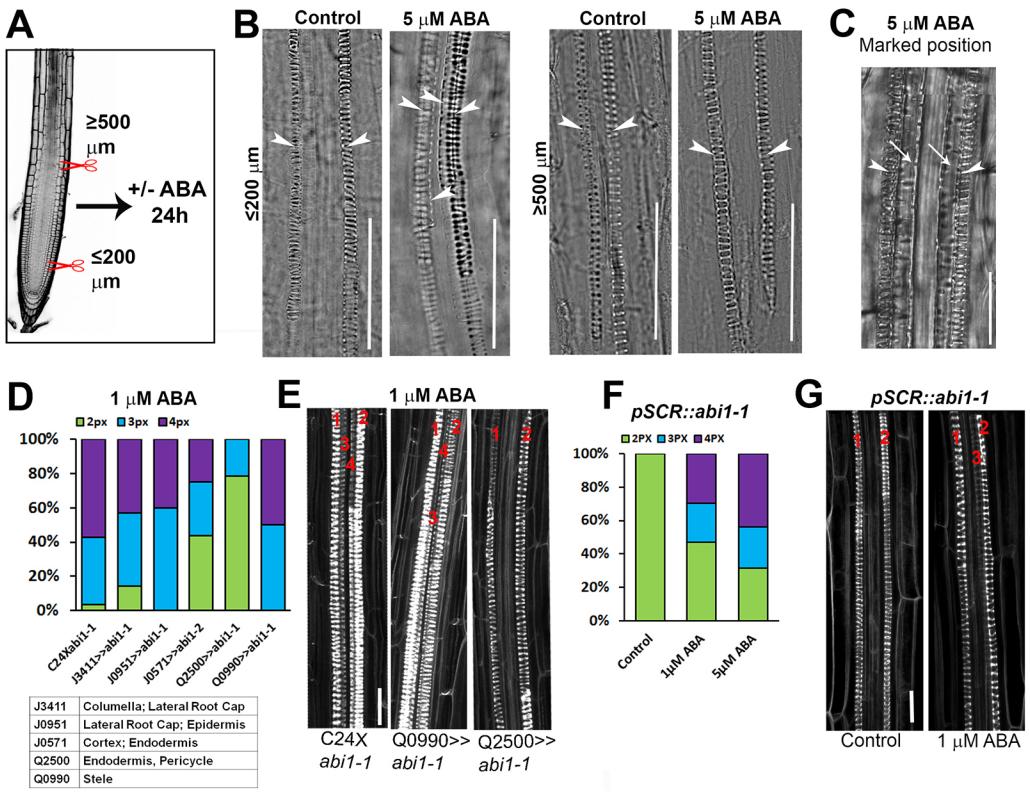

Fig. 3. Endodermal ABA signaling and regenerating competent root meristem cells are required for xylem differentiation of MX provascular cells to PX. (A) Schematic of excision experiments. Roots were excised at distances equal to or below 200 µm (≤200 µm) or equal to or above 500 µm (≥500 µm) from the tip. Xylem development was examined after 24 h. (B) Differential interference contrast (DIC) images of cleared roots following excisions at distances ≤200 µm or ≥500 µm from the tip and subsequent 24 h treatment with control or 5 µM ABA. Arrowheads mark PX. (C) DIC images of vascular tissues after labeling the initiation of the elongation zone and subsequent 24 h treatments with 5 µM ABA. Arrowheads indicate PX, arrows indicate MX. (D) Frequencies of PX files formed in *pUAS::abi1-1* crossed to enhancer trap lines or *C24* background for control in the F1 generation following 24 h in 1 µM ABA. The table specifies the expression pattern of enhancer trap lines in the root (*C24* n=20; *J3411*, *Q2500* and *Q0990* n=14; *J0571* n=16; *J0951* n=10). (E) *z*-stack maximal projection of PI-stained xylem following 24 h 1 µM ABA treatments. Red digits indicate PX cell files. (F) Frequencies of PX formation in *pSCR::abi1-1* line following 24 h ABA treatments (n=16-17 per treatment). (G) *z*-stack maximal projection of PI-stained vascular tissue in *pSCR::abi1-1* seedlings treated with 1 µM ABA or solvent control. Red digits indicate PX cell files. Scale bars: 50 µm in B; 20 µm in C,E,G. See also Figs S8 and S9.

differentiation were reduced in non-aborted *tir1;afb2;afb4;afb5* quadruple auxin receptor mutant roots (Prigge et al., 2016). Conversely, ABA effects were enhanced in *35S::Iaa6m1m2* plants, which display a constitutive auxin response (Li et al., 2011). Moreover, qPCR analysis indicated that a 3 h ABA treatment did not affect RNA levels of three auxin biosynthesis genes, *TAA1*, *YUCCA3* or *YUCCA9*, and caused an ∼2-fold reduction in *YUCCA5* mRNA levels. Taken together, the analysis of ABA-auxin interaction (Figs S11 and S12) indicated that ABA and auxin do not function in the same pathway but rather have synergistic effects on xylem differentiation, providing an explanation for why AHP6 was not upregulated by ABA.

Next, we examined whether ABA affects the expression of *miR165a/166b* and the HD-ZIPIII targets of these miRNAs (De Rybel et al., 2016). ABA treatments induced significant increases in the expression of *pmiR165a::*GFP and *pmiR166b::*GFP (*miR165a/166b*) (Carlsbecker et al., 2010) in the endodermis and cortex, respectively (Fig. 4B,C,G,H and Fig. S10B,C). Similarly, *miR165a* expression was induced by mandipropamid in $PYR1^{MANDI}$ plants (Fig. 4D,I and Fig. S10D), indicating that enhancement of *miR165a* expression involved core ABA signaling. *miR165/166* levels were previously shown to be negatively regulated by ZLL (Liu et al., 2009; Yu et al., 2017; Zhu et al., 2011). In roots of *zll/pZLL::YFP:ZLL* (Tucker et al., 2008) YFP:ZLL is expressed in the stele, with the highest expression in procambial cells and lower levels in xylem cells (Fig. 4E and Fig. S10E). Treatments with 5 µM ABA caused reduction in YFP:ZLL expression levels (Fig. 4E,J and Fig. S10E), likely leading to increased levels of free *miR165a/166b* in the stele. Taken together, ABA increases *miR165a*/*166b* levels by inducing their expression and repressing the expression of their suppressor ZLL.

As *miR165a* and *miR166b* target mRNAs encoding HD-ZIPIII family proteins, including PHB, we asked whether ABA induced an altered expression pattern of $pPHB::GFP_{ER}$ (*PHB*) transcription and *pPHB::PHB-GFP* (PHB) reporters (Miyashima et al., 2011). For accurate observation tissue clearing was used. The expression pattern and levels of *PHB* transcript reporter were similar in control and ABA treatment (Fig. 4K,M and Fig. S10F), indicating that ABA does not influence the transcription of *PHB*. In contrast, ABA treatment resulted in reduction in the levels of PHB protein reporter. In control seedlings, PHB was detected in the central part of stele, excluding the pericycle. Following incubation with ABA, PHB levels were lower and more restricted (Fig. 4L,N and Fig. S10G). Importantly, reduction in PHB levels were already detected following 3 h and 5 h treatments with ABA, suggesting rapid effect of ABA on PHB mRNA levels (Fig. 4O). Taken together, the analyses of ABA signaling with the data on *miR165a/miR165b*, *PHB* and PHB expression indicate that ABA signaling

Development (2019) 146, dev177097. doi:10.1242/dev.177097

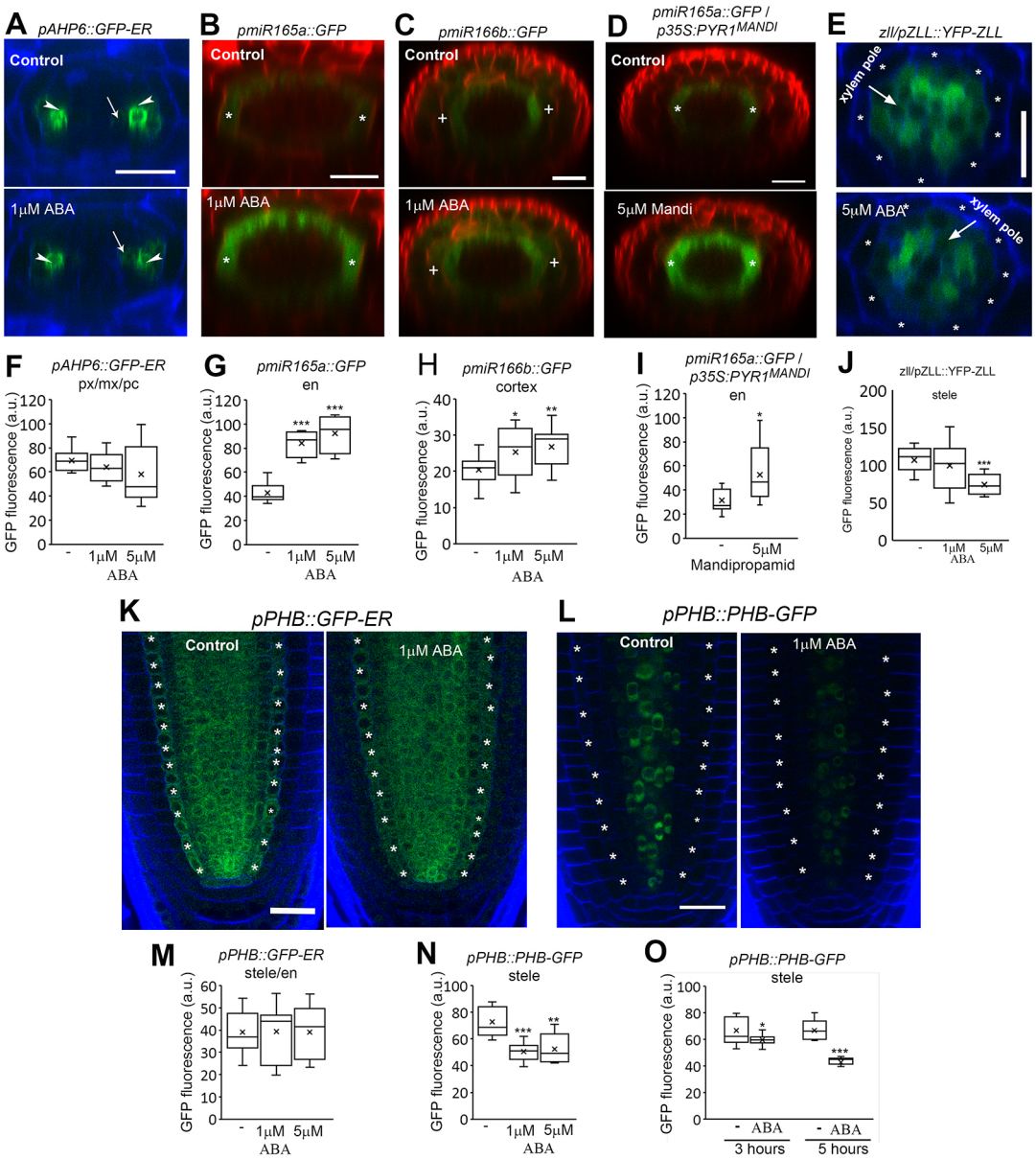

Fig. 4. ABA regulates expression levels and pattern of *miR165a*/*166b* and PHB expression but does not influence *AHP6* expression. (A) *z*-cross-sections of *pAHP6::GFP-ER* expression in root meristem of cleared roots treated for 24 h with solvent control or 1 µM ABA. Note that expression was detected in PX (arrowheads) and at low levels in pericycle and MX (arrows) in both control and ABA-treated seedlings. (B,C) *z*-cross-sections of *pmiR165a::GFP-ER* (B) and *pmiR166b::GFP-ER* (C) in root meristem after 24 h treatments with control or 1 µM ABA. Asterisks indicate endodermis, + indicates cortex. (D) *z*-cross-sections of *pmiR165a::GFP-ER* in *p35S::PYR1^{MANDI}* background after 24 h induction with 5 µM mandipropamid or control. Asterisks indicate endodermis. (E) *z*-cross-sections of *zll/pZLL::YFP-ZLL* (green) cleared root meristem after treatment with control or ABA. Asterisks mark the endodermis. Note low expression levels in the xylem pole in control and a decrease after ABA treatments (arrows). (F-J) Fluorescence intensities of respective reporters after 24 h in control or ABA-containing media: *pAHP6::GFP-ER* in PX, MX and pericycle (*n*=14-18 per treatment) (F); *pmiR165a::GFP-ER* in endodermis (*n*=9 per treatment) (G); *pmiR166b::GFP-ER* in cortex layer (*n*=14 per treatment) (H); *pmiR165a::GFP-ER*/*p35S::PYR1^{MANDI}* in endodermis (*n*=11-14 per treatment) (I); *zll/pZLL::YFP-ZLL* in stele (*n*=14 per treatment) (J). (K,L) Longitudinal sections of cleared roots of *pPHB::GFP-ER* and *pPHB::PHB-GFP* seedlings. Asterisks mark endodermis. (M,N) Quantification of fluorescence intensities of indicated reporters following 24 h in control or ABA-containing media: *pPHB::GFP-ER* in stele and endodermis (*n*=10 per treatment) (M); *pPHB::PHB-GFP* in stele (*n*=12-16 per treatment) (N). (O) *pPHB::PHB-GFP* in stele following 3 h or 5 h treatments with ABA (*n*=10-15 per treatment). ABA concentration 10 µM. In A, I and J cell walls of cleared roots were stained with Calcofluor White (blue). In B-D, staining with PI (red) was performed without clearing. Fluorescence of GFP-based reporters is shown in green. In box plots, x indicates the mean, the line indicates the median, the box indicates lower quartile (Q1) and upper quartile (Q3), whiskers indicate lowest and highest values. *P≤0.05; **P≤0.005; ***P≤0.0005, Student's *t*-test, two-tail distribution, unequal variance. Scale bars: 20 µm. See also Figs S10, S11 and S12.

in endodermal precursors induces expression of *miR165a/166b* and reduces the level of their negative regulator ZLL, and that these miRNAs post-transcriptionally repress the expression of *PHB* and possibly other HD-ZIPIII-encoding genes in meristematic cells.

Inhibition of lateral root emergence by ABA correlates with increased expression of *miR165a* and a consequent reduction in PHB levels and spatial distribution

Previous findings on the role of primary root endodermis ABA signaling in inhibition of LR growth (Duan et al., 2013) promoted

Development (2019) 146, dev177097. doi:10.1242/dev.177097

us to examine whether, and how, ABA regulates *miR165a* and PHB during LR development. Weak expression of *miR165a* in cleared roots was first detected at stage IV in outer layer 2 precursors of endodermis, cortex and QC (Fig. 5A) of lateral root initials (LRIs), in which SCR is expressed (Goh et al., 2016). *miR165a* expression increased in a linear fashion up to the emergence stage and then an exponential increase in *miR165a* expression was detected at the post-emergent LRIs (Fig. 5A,B). At stage VII, and more significantly at the emergence and post-emergence stages, *miR165a* expression dropped down in QC precursor cells and was restricted to endodermal precursors (Fig. 5A, white arrows). Treatments with 1 µM ABA significantly increased *miR165a* expression levels specifically at the emergence and post-emergence stages, coinciding with the ABA-induced LR quiescence at emergence stage (De Smet et al., 2003) (Fig. 5A,B). Furthermore, the ABA treatments also inhibited the reduction in

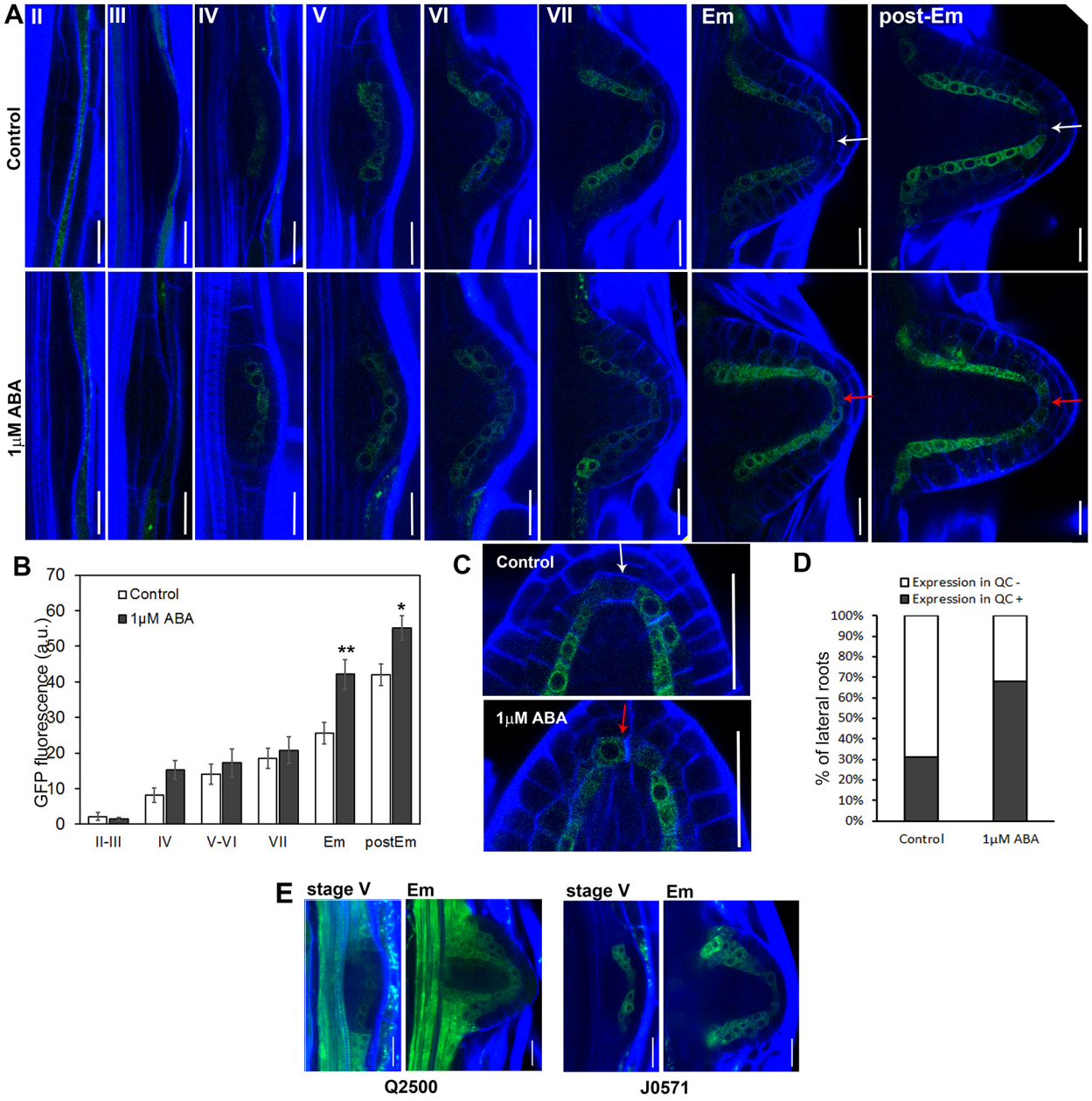

Fig. 5. ABA upregulates *miR165a* expression in lateral root initials specifically at the emergence stage. (A) Expression of *pmiR165a::GFP-ER* at different stages of LR development in cleared roots treated for 24 h with control or 1 µM ABA. (B) Quantification of *pmiR165a::GFP-ER* fluorescence intensities in outer layer 2 at stages II-VI and in endodermis precursor cells at stage VII, emergence and post-emergence (*n*=25/16 stages II-III; *n*=25/16 stage IV; *n*=24/19 stages V-VI; *n*=14/13 stage VII; *n*=26/27 emergence and *n*=20/19 post-emergence, in control/ABA respectively). (C) *pmiR165a::GFP-ER* expression in QC precursor cells at emergence stage. (D) Frequencies of *pmiR165a::GFP-ER* expression in QC precursor cells at the emergence stage with and without ABA treatments (control *n*=26; ABA-treated *n*=27). (E) Expression of stele/endodermis and cortex/endodermis-specific *pUAS::abi1-1* lines *Q2500* and *J0571*, respectively, in cleared LR initials at stage V and emergence. Cell walls were stained with Calcofluor White (blue). The activity domain of GAL4 enhancer trap lines was visualized by GFP (green). In A, C and E, cell walls of cleared roots were stained with Calcofluor White (blue). GFP (green). White and red arrows mark the position of QC precursor cells in control and ABA-treated roots, respectively. Em, emergence stage. Data are mean±s.e.m. **P*≤0.05; ***P*≤0.005, Student's *t*-test, two-tail distribution, unequal variance. Scale bars: 50 µm in A; 20 µm in C,E. See also Fig. S13.

Development (2019) 146, dev177097. doi:10.1242/dev.177097

miR165a levels in the QC precursor cells (Fig. 5C,D). Importantly, enhancer trap lines *Q2500* and *J0571*, which drive the expression of abi1-1 in the primary root endodermis (Duan et al., 2013; Fig. S9) were detected in endodermis and QC precursor cells in LRIs (Fig. 5E). Thus, it is highly likely that inhibition of ABA-induced LR quiescence in enhancer trap lines *Q2500* and *J0571* (Duan et al., 2013) was associated with expression of abi1-1 in LRI endodermal precursor cells rather than the endodermis of the main root. It has been shown that ABA inhibits LR growth following emergence, likely through an auxin-independent mechanism (De Smet et al., 2003). Thus, there is a tight correlation between the endodermal/QC precursor cell ABA signaling-induced quiescence of LR growth and the increase in *miR165a* levels specifically at the LRI emergence stage.

In agreement with previously published data (Hawker and Bowman, 2004), PHB expression was already detected in the inner layer (IL) of stage II LRIs and in the progeny of this layer during later stages of LR development in cleared roots (Fig. 6A). Coinciding with the increase in *miR165a* levels, the expression domain of PHB became confined to up to five layers of IL progeny cells in the mid region of emergence stage LRI and restricted from endodermal and pericycle layers (Fig. 6B,D, region 2). Hence, PHB and *miR165a* form complementary expression domains in developing LRIs. Following ABA treatments and coinciding with the increase in *miR165a* levels, the overall levels and the number of cells that express PHB were reduced at the emergence stage (Fig. 6B-D). Taken together, these results strongly suggest that ABA may regulate post-emergent LR growth by regulating the levels of *miR165a*, and hence PHB. *VND7* expression was first detected at post-emergence LRIs but became expanded only in LRs (Fig. 4E), suggesting that PHB likely inhibits *VND7* expression during early LRI development.

To further examine function of HD-ZIPIII in LR development we examined the root length and LR development in a triple *phb;phv;cna* mutant (Prigge et al., 2005) and LR development in the gain-of-function *phb1-d* mutant (McConnell et al., 2001). Following treatments with 0.5 µM ABA, root lengths of *Col-0* and *phb;phv;cna* were significantly reduced ($P \leq 0.005$, Student's *t*-test). Interestingly, following ABA treatment the *phb;phv;cna* were slightly but significantly shorter ($P \leq 0.05$. Student's *t*-test) (Fig. S13A). The ABA treatments caused significant reduction in LR density in both *Col-0* and the *phb;phv;cna* seedlings ($P \leq 0.005$, Student's *t*-test) but no differences were detected between the WT and mutant plants (Fig. S13B). *phb1-d* mutants developed very short primary roots, with seedlings developing not more than one LR under control conditions. Interestingly, some *phb1-d* seedlings developed a LR following a treatment with 1 µM ABA (Fig. S13C). However, owing to the short primary root length and the very small number of LR it is difficult to know whether the development of LR at 1 µM ABA did indeed reflect a lower sensitivity of the mutant to the hormone during LR development.

Regulation of HD-ZIPIII gene expression by ABA

Quantitative RT-PCR analyses were carried out to examine whether ABA regulates the expression of all five HD-ZIPIII-encoding genes. *PYL4* and *PP2C* are known to be down- and upregulated by

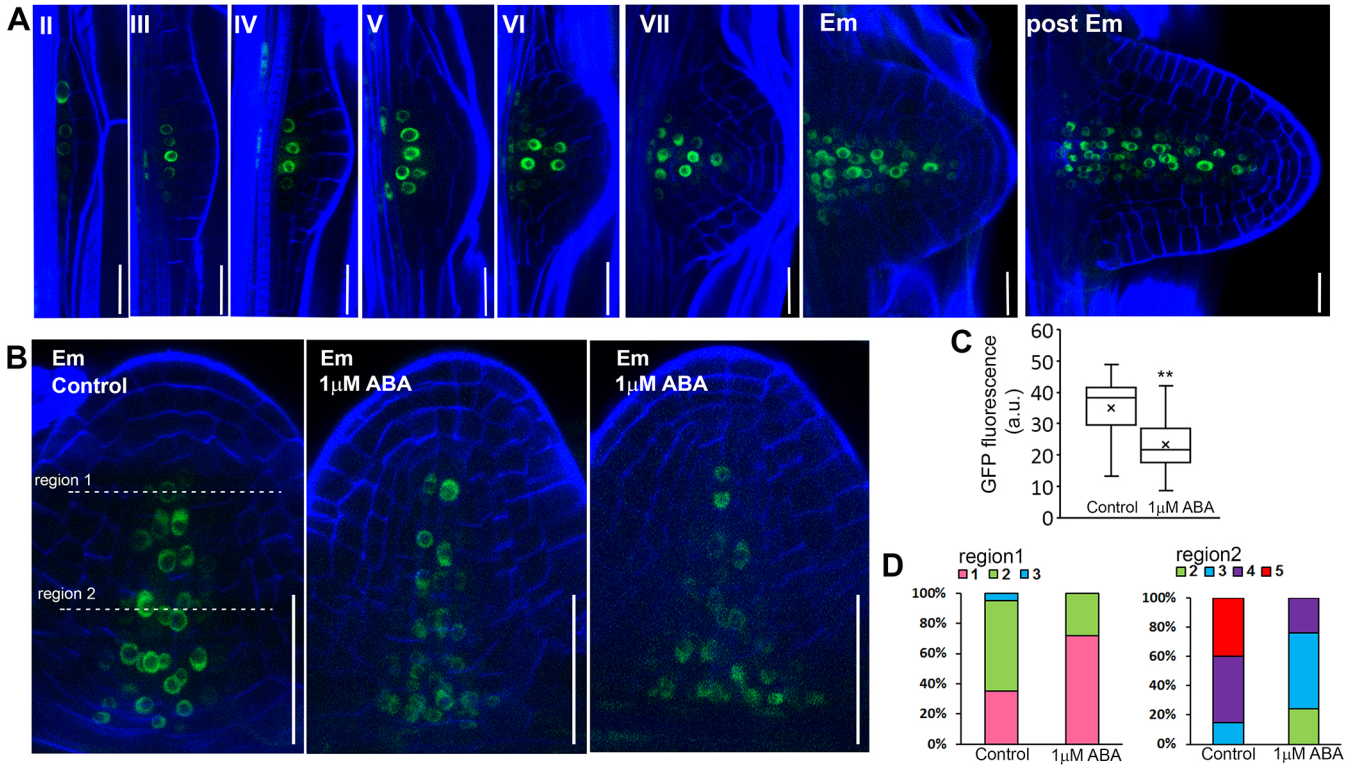

Fig. 6. ABA downregulates and restricts PHB expression in emerging LR. (A) *pPHB::PHB-GFP* expression at defined stages of LR development. (B) *pPHB::PHB-GFP* expression at the emergence stage in control LR or those treated with 1 µM ABA for 24 h. The dashed lines define regions that were used for the quantification presented in D. (C) Quantification of fluorescence intensities in stele following 24 h in control or ABA-containing media. Box plots: x indicates the mean, the line indicates the median, the box lower quartile (Q1) and upper quartile (Q3), whiskers indicate lowest and highest values. (D) Frequencies of number of positive λ cell files in stele in regions 1 and 2. A and B are *z*-stack maximal projections; blue, Calcofluor White; green, GFP. In C and D, control n=20, ABA-treated n=26. Em, emergence stage. **$P \leq 0.005$, Student's *t*-test, two-tail distribution, unequal variance. Scale bars: 20 µm. See also Fig. S13.

Development (2019) 146, dev177097. doi:10.1242/dev.177097

exogenous ABA treatments, respectively, and were used as controls in all the experiments for monitoring the efficiency of the ABA and mandipropamid treatments (Fig. S14A-C). In *Col-0* seedlings, a 1 h 10 µM ABA treatment resulted in significant reductions in the levels of all five HD-ZIPIII-encoding genes (Fig. 7A). Similarly, a 3 h treatment of *PYR1*^{MANDI} plants with mandipropamid induced significant reductions in the levels of all five mRNAs (Fig. 7B). Furthermore, the effects of ABA on mRNA levels of all five HD-ZIPIII genes were reduced in *abi1-1* and *pyr1;pyl1;pyl2;pyl4* ABA signaling mutants compared with effects in the WT seedlings (Fig. 7C,D). The changes in expression levels of all 5 HD-ZIPIII genes at 24 h were statistically significant, but reduced compared with the 1 h treatment (Fig. S14D). The quantitative RT-PCR data indicated that elevated ABA levels induce a rapid decrease in HD-ZIPIII-encoding mRNAs via core ABA signal transduction, in line with the changes in expression levels of PHB-GFP and *miR165a/166b*. In summary, the developmental and expression analyses indicated that, upon drought stress, increases in ABA levels lead to increases in *miRNA165a/166b*, which cause repression of all five HD-ZIPIII mRNAs. The reduction in the levels of HD-ZIPIII proteins lead in turn to earlier differentiation of MX provascular cells into PX in primary root and likely quiescence at the emergence stage in LRI.

The effects of ABA are repressed in a *miR165/166*-resistant *PHB* mutant and enhanced in a *phb;phv;can* HD-ZIPIII triple mutant

The phenotypes of a *phb1-d* (McConnell et al., 2001) mutant and a triple *phb;phv;cna* (Prigge et al., 2005) mutant with and without ABA treatments were analyzed to further examine the causal relationships between ABA signaling and the timing of SCW formation in PX and endodermis. Basic Fuchsin staining of *phb;phv;cna* roots indicated that the position of PX lignification is not significantly different from that of WT roots (Fig. S15A,B). *phb1-d* is a *miR165a/166b*-resistant mutant and should therefore display reduced sensitivity to ABA (Carlsbecker et al., 2010; Miyashima et al., 2011). Staining of *phb1-d* showed that mutant seedlings generally lack PX and that lignification of MX initiates 17 to 18 cells from the ETZ (Fig. S15A,B). About 10% of *phb-1d* seedlings developed one file of PX at distance of 7 to 8 cells from the ETZ (Fig. S15D). Cases of normal PX development in *phb1-d* have been reported previously (Miyashima et al., 2011). Thus, the PHB gain-of-function in *phb1-d* reduces but does not eliminate PX differentiation. In agreement, treatment of *phb1-d* seedlings with 1 µM ABA resulted in PX development and lignification 6 to 7 cells from the ETZ, indicating that ABA partially overcomes the *miR165a/166b*-resistant phenotype of *pbh1-d* plants (Fig. S15A,B). SCR and SHR regulate the expression of *miR165a/166b* and, similar to *phb1-d*, *scr-3* and *shr-2* mutant plants lack PX and develop MX also in the PX and pericycle cell files (Carlsbecker et al., 2010). Similar to *phb1-d*, MX differentiation takes place later in development and not where PX normally differentiates (Fig. S16A). These data suggest that when cells are not specified as PX they can undergo differentiation into MX later in their development. In both *scr-3* and *shr-2*, PX differentiation could be rescued by treatments with 5 µM ABA, suggesting that ABA-induced increases in *miR165a/166b* levels are partially additive to SHR and SCR (Fig. S16A,B).

Interestingly, whereas SCW lignification in the MX of most *phb1-d* roots takes place 17 to 18 cells from the ETZ, the lignification of the CS in the endodermis occurs 8 cells from the ETZ, even earlier then in *Ler* roots (10 cells from the ETZ) (Fig. S15C,E). Thus, SCW formation in xylem and the CS are genetically separable. In contrast to *Ler* seedlings, the MX of *phb1-d* was visible with PI staining (Fig. S15E), indicating that maturation of the CS is compromised (Roppolo et al., 2011) and suggesting that PHB influences CS integrity.

In *Ler* roots, ABA induced formation of four PX files, but at lower frequencies compared with *Col-0*. In *phb-1d* roots, following ABA treatments no, one, two and rarely three PX files, but not four PX files, were observed (Fig. 8A,B,E). In *scr-3* and *shr-2*, ABA induced the formation of only one or two PX files (Fig. 8D,E). Thus, in the *miR165a/166b*-resistant *phb1-d*, as well as in *scr-3* and *shr-2* roots, the effects of ABA were suppressed compared with WT. Conversely, ABA enhanced PX formation in the *phb;phv;cna* triple mutant, resulting in formation of five and six PX files (Fig. 8C,E).

We hypothesized that ABA-induced reductions in the levels of *PHV*, *REV*, *CNA* and *ATHB8* partially overcome the *phb1-d* gain-of-function and enable differentiation of PX. qPCR was used to examine the expression of all five HD-ZIPPIII genes in *phb1-d*. As expected, *PHB* RNA levels are significantly increased in *phb1-d* compared with *Ler*. Interestingly, the levels of *ATHB15*, *ATHB8* and *PHV* were also increase relative to *Ler* (Fig. S14E). In ABA-treated *Ler* seedlings, all five HD-ZIPIII RNA levels were reduced (Fig. 8F), indicating that ABA had a similar effect on HD-ZIPIII expression in *Ler* and *Col-0* ecotypes. In ABA-treated *phb1-d* seedlings, levels of *PHV*, *REV* and *ATHB8* RNAs were reduced compared with control, whereas *PHB* and also *ATHB15* RNA levels were not affected by the ABA treatments (Fig. 8G).

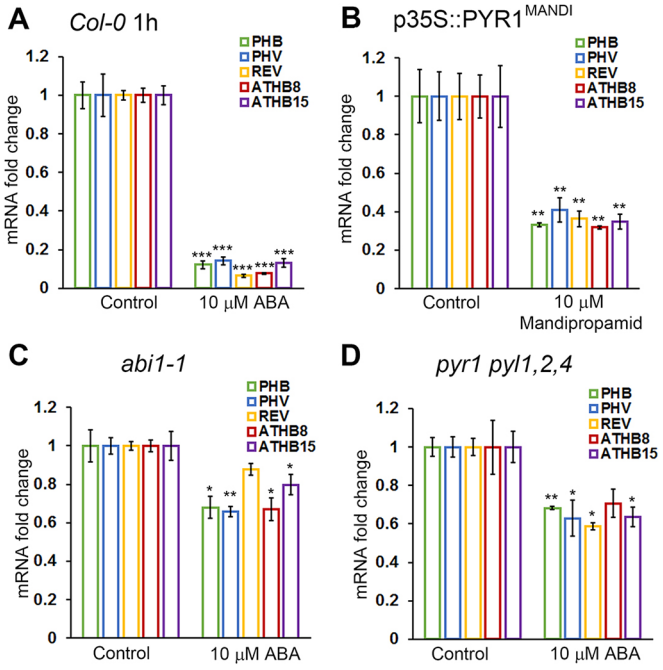

Fig. 7. ABA downregulates expression of HD-ZIPIII-encoding mRNAs. (A-D) Quantitative RT-PCR analyses of transcript levels in roots were determined; fold changes relative to appropriate control seedlings are plotted. Expression of indicated transcripts in *Col-0* seedlings after 1 h treatment with 10 µM ABA (A); expression of indicated transcripts in *p35S::PYR1*^{MANDI} after 3 h treatment with 10 µM mandipropamid (B); expression of indicated transcripts in *abi1-1* (C) and *pyr1;pyl1;pyl2;pyl4* (D) seedlings after 1 h treatment with 10 µM ABA. **P*≤0.05; ***P*≤0.005; ****P*≤0.0005, Student's *t*-tests, two-tail distribution, unequal variance. Data are mean±s.e.m. See also Fig. S14.

DISCUSSION

ABA has been referred to as 'the hidden architect of root structure' (Harris, 2015). The general effect of ABA on the root is the

Development (2019) 146, dev177097. doi:10.1242/dev.177097

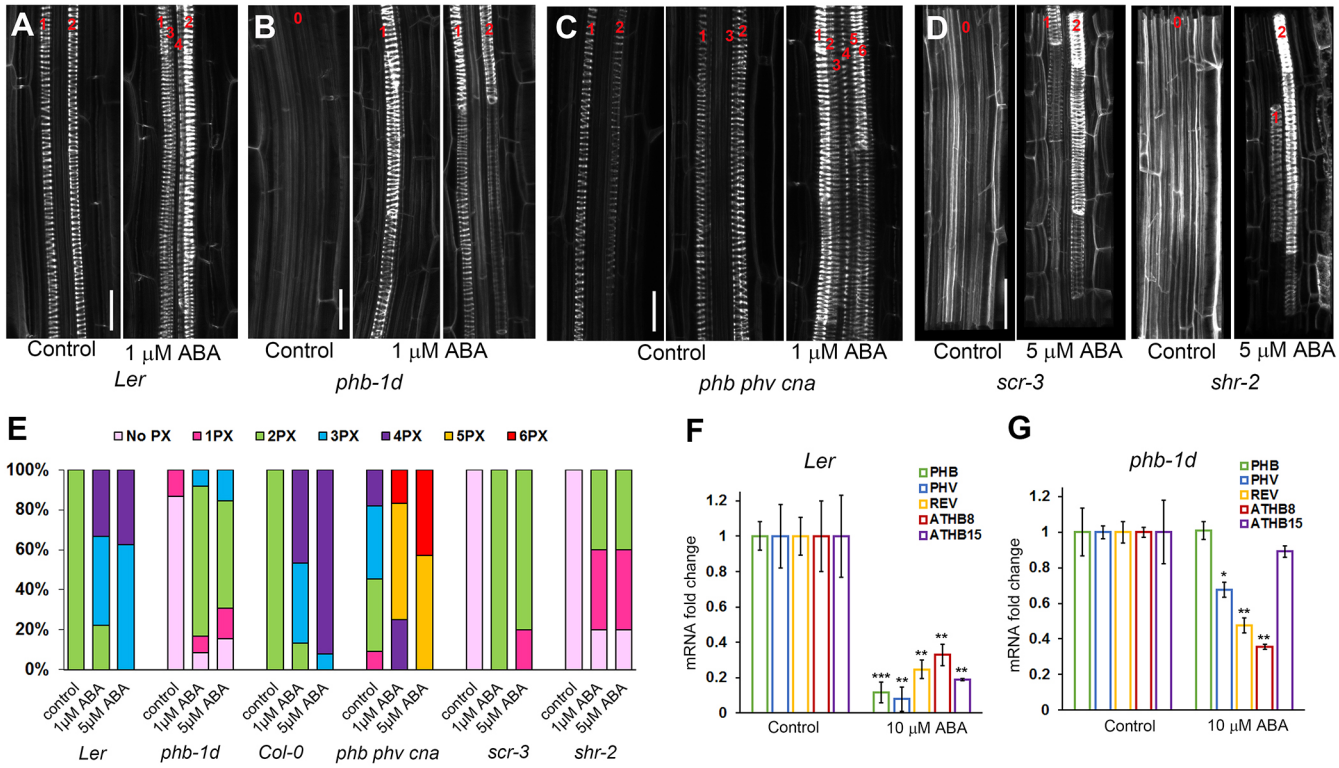

Fig. 8. ABA rescues PX specification in *phb-1d* but differentiation of MX to PX is suppressed or enhanced in *phb-1d* and *phb;phv;cna* roots, respectively. (A-C) Representative *z*-stack maximal projections of vascular tissues stained with PI (white) at distance of 11 to 13 cells from ETZ of *Ler*, *phb1-d* and *phb;phv;cna* roots following incubation in control or 1 µM ABA-containing media for 24 h. (D) Representative 3D reconstruction of vascular tissue in *scr-3* and *shr-2* with and without 5 µM ABA. Red digits (A-D) indicate PX cell files. (E) Frequencies of PX in *Ler*, *phb-1d*, *Col-0*, *phb;phv;cna*, *scr-3 and shr-2* roots with and without ABA treatments (*Ler* n=9; *phb-1d* n=12-15; *Col-0* n=13-15; *phb;phv;cna* n=11-12; *scr-3* n=5-7; *shr-2* n=5 per treatment). (F,G) qPCR analysis of relative transcript levels of HD-ZIPIII mRNAs in roots of *Ler* (F) and *phb-1d* (G) treated for 2 h with 10 µM ABA. Data are mean±s.e.m. *P≤0.05; **P≤0.005; ***P≤0.0005, Student's *t*-tests, two-tail distribution, unequal variance. Scale bars: 20 µm. See also Figs S14E, S15 and S16.

enhancement of maturation, which is reflected in smaller cell number in the cell division and elongation zones, premature differentiation of PX and maturation of the CS. ABA regulates PX differentiation and likely LR emergence by regulating the levels of *miR165a/166b* (Fig. 9).

Similarly, it has been shown that osmotic stress induces formation of additional PX files via endodermal ABA signaling that enhances the expression of *miR165a*, thereby reducing RNA levels of all five HD-ZIPIII RNAs (Ramachandran et al., 2018). The same work also demonstrated that ABA is required for the continuity of the MX files. Our work adds several essential and distinctive findings. By analyzing both *Arabidopsis* and tomato roots we show that the primary effect of ABA is the timing of PX maturation, by affecting the levels of *VND7* expression in provascular cells. This finding suggests that commitment of MX provascular cells to differentiate into MX takes place later in development and that in the meristem these cells maintain the plasticity to differentiate into PX. VND7 represses the expression of *REV* and *PHB* by directly binding to their promoters. REV represses *PAL4*, suggesting that VND7 induces expression of SCW genes by suppressing the expression of HD-ZIPIII proteins (Taylor-Teeples et al., 2015). The analysis of tomato roots also showed that the effect of ABA on xylem differentiation are evolutionarily conserved. In addition, we identified ABA receptors that are involved in regulating xylem differentiation.

Uniquely we show that ABA also affects *miR165a/166b* by regulating the expression level of their suppressor ZLL. High expression levels of ZLL in the procambium likely reduced the levels of free *miR165a/166b* in procambial cells, restricting their inhibitory effect to the xylem pole. Similarly, in the shoot meristem, ZLL is required for maintaining the stem cell niche and leaf polarity through suppression of *miR165/166* expression (Liu et al., 2009; Tucker et al., 2008).

We have not observed expansion of the *AHP6* expression domain by ABA, contrary to Ramachandran et al. (2018). Using clearing, we observed *AHP6* expression outside the PX files in control untreated plants. Our results agree with the additive effects of ABA and auxin in PX differentiation, which indicate that ABA does not affect xylem differentiation via core auxin signaling. The analysis of ABA effects in the *shr* and *scr* background indicated that its effects are partially independent of their function. Our results also indicate that ABA regulates *miR165/166* levels in endodermal precursor cells in both primary roots and LRIs.

It has been shown that SCR is required for the establishment of LR QC (Goh et al., 2016). Consistently, we discovered a specific expression pattern of *miR165a* in LRIs, which is regulated by ABA at the emergence stage, when ABA suppresses LR growth. These findings provide a possible mechanism for earlier findings on the non-cell autonomous role of endodermal ABA signaling which regulates LR growth (Duan et al., 2013). Alternatively, the ABA-induced upregulation of *miR165a* in the QC may be a consequence of a specific effect on LR meristem formation.

Our finding demonstrate that ABA regulates xylem patterning, CS maturation and possibly LR emergence via *miR165/166* and

Development (2019) 146, dev177097. doi:10.1242/dev.177097

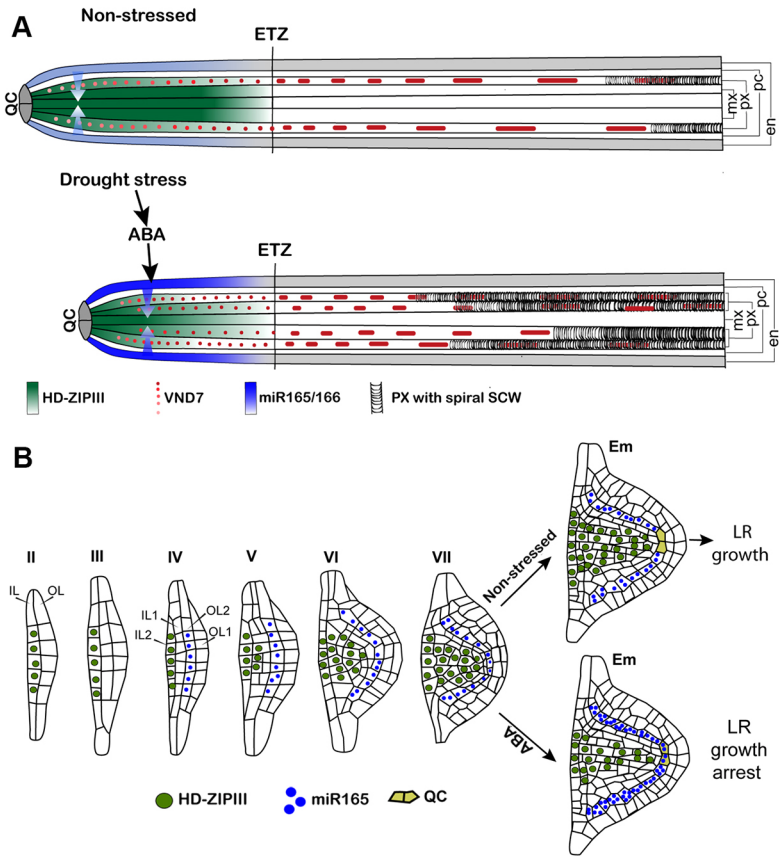

Fig. 9. A graphical summary of the major findings. (A) Illustrations showing stele and surrounding endodermis. In the absence of drought stress (top), *miR165a*/*166b* expressed in the endodermis (light blue gradient arrows) enter the stele where they reduce HD-ZIPIII levels in the central part of the stele (green gradient). *VND7* levels increase gradually (red nuclei) specifying differentiation of SCW at a distance of 8 to 9 cells from the end of transition zone (ETZ). During drought stress (bottom), ABA acts on endodermis in the cell division zone causing upregulation of *miR165*/*166* expression (dark blue arrows). High levels of *miR165a*/*166b* repress HD-ZIPIII in the xylem pole, inducing rapid increase and the spreading of *VND7* expression that results in faster differentiation of PX (5 to 6 cells from ETZ) and differentiation of MX precursors to PX. The intensities of light/dark blue, green and red colors correspond to the levels of *miR165a*/*166b*, HD-ZIPIII and VND7, respectively. (B) The expression patterns and levels of *miR165a* and PHB during LR development and the changes in their expression at the emergence stage following ABA treatments. Number of blue circles represents the intensity of *miR165a* expression. Green circles represent the distribution of PHB:GFP expression. Em, emergence stage LRI; en, endodermis; IL, inner layer; mx, metaxylem; OL, outer layer; pc, pericycle; px, protoxylem; QC, quiescent center.

HD-ZIPIII levels, and that ABA regulation of xylem differentiation is evolutionarily conserved.

MATERIALS AND METHODS

Plant materials and growth conditions

Arabidopsis plants used in this study were in *Col-0*, *Ler* or *C24* ecotypes. Analysis of *abi1-1* enhancer trap lines and *p35S::PYR1*^{MANDI} and *pMIR165a::GFP* crosses were carried out at the F1 generation. Plants were grown on 0.5× Murashige & Skoog (MS) salt mixture plates under long-day conditions (16 h light/8 h dark). For more details, see supplementary Materials and Methods. See Table S2 for resources.

Hormone and drug treatments

Seedlings at 5 days after germination (DAG) or 12 DAG (for lateral root experiments) were transferred under sterile conditions to fresh standard plates supplemented with +(-)cis, trans-abscisic acid (ABA; Duchefa A0941, 10 mM stock solution in ethanol); mandipropamid (Sigma-Aldrich, 32805, 10 mM stock solution in methanol); α-naphthaleneacetic acid (NAA; Sigma-Aldrich, N-0640, 100 mM stock in ethanol), auxinole (a gift from Ken-Ichiro Hayashi, Okayama University of Science, Japan, 50 mM in DMSO). For control treatments, plates were supplemented with solvents alone. All analyses were carried out 24 h after transfer to the new growth conditions.

PEG800, NaCl and sorbitol treatments

Five DAG seedlings were transferred to standard plates supplemented with NaCl, sorbitol or PEG 8000 (Sigma-Aldrich, P5413) at indicated concentrations. PEG 8000-infused plates were prepared according to a previously described procedure (Verslues et al., 2006). In brief, plates containing 20 ml of standard agar media were covered with 30 ml liquid 0.5× MS media supplemented with PEG 8000 and incubated overnight at room temperature. To obtain final concentrations of 60 g/L and 120 g/L, plates were covered with 100 g/L and 200 g/L PEG 8000, respectively. The 500 g/L PEG 8000 stock solution in 0.5× MS media was filter sterilized and stored at 4°C in the dark. Liquid PEG 8000 media were removed just before seedling transfer, and plates were sealed with paraffin and transferred to growth chamber for 24 h. Importantly, for reproducible results, the PEG 8000 was freshly prepared. All analyses were carried out 24 h after transfer to the new growth conditions.

Root staining with PI and imaging

Seedlings were stained for 10 min with 100 µg/ml PI (Sigma-Aldrich, P4864, 1 mg/ml in doubly distilled water), washed for 1 min in water, and immediately subjected to imaging.

Cell length measurements

Roots were stained with PI. Cell length measurements were carried out using the semi-automated Cell-o-Tape macro for ImageJ (Fiji) (Band et al., 2012). All measurements were taken from the cortex cell layer, with numbering starting from the first initial adjacent to the QC. For more details see supplementary Materials and Methods.

Analysis of xylem morphology

Analyses were carried out on roots stained with PI, at a constant region in the maturation zone of the root, 3 or 4 cells distal from the first emerging root hair or 11 to 13 cells from ETZ. In control conditions, maturing PX cells at this region have a well-defined spiral pattern and MX differentiation could not be detected. Confocal imaging of vascular tissue was carried out using a Zeiss C-Apochromat 40×/1.20 W objective. The number of PX cell files was evaluated by 3D reconstruction (ZEN software, Zeiss) of *z*-stack confocal sections. Typical stacks consisted of 25-30 sections at 0.6 µm intervals.

Clearing and staining of roots

Roots were fixed in 4% paraformaldehyde and cleared in ClearSee reagent for 1 week according to the published protocol (Kurihara et al., 2015). Tomato roots were fixed and cleared with ClearSee for 1 month. Primary cell walls were stained with Calcofluor White (100 µg/ml in ClearSee, Sigma-Aldrich, 18909) for 1 h at room temperature and washed overnight in

ClearSee solution. For double staining with Calcofluor White and basic Fuchsin (Fluka, 47860), cleared seedlings were incubated in basic Fuchsin (0.05% w/v in ClearSee) for 24 h, washed for 1 h in ClearSee, then stained with Calcofluor White (100 µg/ml in ClearSee) for1 h, washed for 24 h in ClearSee solution, and mounted on slides in ClearSee. The staining of tomato roots was similar, except the incubation with Calcofluor White and basic Fuchsin was carried out for 24 h.

Quantification of PX, MX and CS lignification position in roots

For quantification of PX, MX and CS lignification position, cleared roots were double stained with Calcofluor White and basic Fuchsin. Images were captured using a C-Apochromat 40×/1.20 W objective, 8-bit depth (Zeiss). Zeiss Plan-Apochromat 20×0.8 M27 objective was used for image acquisition of tile-scans in the middle sections of roots. Counts were done on cortex cells stained with Calcofluor White, from the ETZ to the position of first PX, MX or CS stained by basic Fuchsin. Fluorescence intensity in appropriate cell layers, as indicated in the text, was measured using Fiji.

Root excisions

Roots of *DR5::Venus-NLS* 5 DAG seedlings were excised under a dissecting microscope as previously described (Sena et al., 2009). Sectioning was carried out either 500-600 µm from root tip (complete removal of root meristem including QC, division and transition zones) or 150-200 µm from the tip (removal of QC and first initials in the division zone). After excision, seedlings were immediately transferred to 0.5× MS, 1% sucrose and 0.8% agar plates supplemented with 5 µM ABA or 0.1% ethanol for control, grown vertically for 24 h, and cleared with ClearSee.

Root labeling

Immediately after transfer to fresh plates, the position of the elongation zone in each root (*Col-0*) was labeled by placing a small granule of coal on the agar close to the root. Seedlings were grown vertically for 24 h, then the section of the root below the coal was removed and the upper root region was transferred to the clearing solution and subsequently analyzed.

Analysis of lateral roots

12 DAG roots were transferred to standard plates supplemented with 1 µM ABA or solvent for 24 h, cleared and stained with Calcofluor White. Stages of LR development were determined according to Malamy and Benfey (1997).

Confocal microscopy

Images were captured on Zeiss LSM 780-NLO laser-scanning confocal microscope. Image analyses were performed using Fiji and Zeiss ZEN10. Where necessary, channel dye separation was used for separating signal from autofluorescence. For more details, see supplementary Materials and Methods.

Time-lapse imaging and quantification of DII-Venus expression levels

DII-Venus-NLS seeds were germinated and grown in 24-well plates on 0.5× MS, 1% sucrose and 0.8% agar medium for 5 days at an angle of 35° to enable roots to reach the bottom of the wells and continue growing between the medium and the bottom of the plate. ABA (5 µM), auxinole (25 µM) or DMSO was added to wells, and time-lapse imaging of root tips was carried out using Zeiss LD Plan-Neofluar 40×/0.6 objective for 80 min, with 5 min intervals, on 8-bit depth single confocal sections. Mean fluorescent intensity in root tips was quantified for each time point using Fiji (ImageJ). Fold change in fluorescence intensity was calculated compared with time point 0. Mean fold changes are based on measurements carried out on five or six seedlings per treatment.

Quantification of marker expression levels in root meristem

Images were captured using a C-Apochromat 40×/1.20 W objective, 8-bit depth. Fluorescence intensity in appropriate cell layers, as indicated in text, was measured using Fiji.

Gene expression by quantitative RT-PCR

Total RNA was extracted from roots and used for reverse transcription, which was in turn used for qPCR (see Table S1 for primers). At least three biological replicates were used for each genotype and treatment, and representative experiments are presented in figures. For more details, see supplementary Materials and Methods.

Quantifications and statistical analyses

Stacked charts and box plots were prepared using Office Excel 2016. Statistically significant differences were determined using the Student's *t*-test, two-tail distribution, unequal variance. The *n* values, which represent different roots, and precision measures are specified in figures and figure legends.

Acknowledgements

We thank Annelie Carlsbecker, Keiji Nakajima, Sean Cutler, Philip Benfey, José Dinneny, Thomas Laux, John Bowman, Eilon Shani, Mark Estelle and Tako Demura for materials, and Eilon Shani, José Dinneny and members of the Yalovsky lab for helpful comments and discussions.

Competing interests

The authors declare no competing or financial interests.

Author contributions

Conceptualization: D.B., S.Y.; Methodology: D.B., M.R.P., A.M.; Validation: D.B., S.Y.; Formal analysis: D.B., M.R.P., A.M., S.Y.; Investigation: D.B., M.R.P., S.Y.; Resources: A.M.; Data curation: D.B., S.Y.; Writing - original draft: D.B., S.Y.; Writing - review & editing: D.B., S.Y.; Visualization: D.B., M.R.P., S.Y.; Supervision: S.Y.; Project administration: S.Y.; Funding acquisition: S.Y.

Funding

This research was supported by the Israel Science Foundation (ISF 827/15, ISF-NCSF 1125/13, ISF-UGA 2739/16) and the Israeli Centers for Research Excellence on Plant Adaptation to Changing Environment (I-CORE 757-12) through grants to S.Y. and by the Mana Center for Plant Research at Tel Aviv University.

Supplementary information

Supplementary information available online at
http://dev.biologists.org/lookup/doi/10.1242/dev.177097.supplemental

References

Antoni, R., González-Guzmán, M., Rodriguez, L., Peirats-Llobet, M., Pizzio, G. A., Fernandez, M. A., De Winne, N., De Jaeger, G., Dietrich, D., Bennett, M. J. et al. (2013). PYRABACTIN RESISTANCE1-LIKE8 plays an important role for the regulation of abscisic acid signaling in root. *Plant Physiol.* **161**, 931-941. doi:10.1104/pp.112.208678

Audran, C., Borel, C., Frey, A., Sotta, B., Meyer, C., Simonneau, T. and Marion-Poll, A. (1998). Expression studies of the zeaxanthin epoxidase gene in nicotiana plumbaginifolia. *Plant Physiol.* **118**, 1021-1028. doi:10.1104/pp.118.3.1021

Band, L. R., Wells, D. M., Larrieu, A., Sun, J., Middleton, A. M., French, A. P., Brunoud, G., Sato, E. M., Wilson, M. H., Peret, B. et al. (2012). Root gravitropism is regulated by a transient lateral auxin gradient controlled by a tipping-point mechanism. *Proc. Natl. Acad. Sci. USA* **109**, 4668-4673. doi:10.1073/pnas.1201498109

Bishopp, A., Help, H., El-Showk, S., Weijers, D., Scheres, B., Friml, J., Benková, E., Mähönen, A. P. and Helariutta, Y. (2011). A mutually inhibitory interaction between auxin and cytokinin specifies vascular pattern in roots. *Curr. Biol.* **21**, 917-926. doi:10.1016/j.cub.2011.04.017

Carlsbecker, A., Lee, J.-Y., Roberts, C. J., Dettmer, J., Lehesranta, S., Zhou, J., Lindgren, O., Moreno-Risueno, M. A., Vatén, A., Thitamadee, S. et al. (2010). Cell signalling by microRNA165/6 directs gene dose-dependent root cell fate. *Nature* **465**, 316-321. doi:10.1038/nature08977

Dello Ioio, R., Galinha, C., Fletcher, A. G., Grigg, S. P., Molnar, A., Willemsen, V., Scheres, B., Sabatini, S., Baulcombe, D., Maini, P. K. et al. (2012). A PHABULOSA/cytokinin feedback loop controls root growth in Arabidopsis. *Curr. Biol.* **22**, 1699-1704. doi:10.1016/j.cub.2012.07.005

De Rybel, B., Mahonen, A. P., Helariutta, Y. and Weijers, D. (2016). Plant vascular development: from early specification to differentiation. *Nat. Rev. Mol. Cell Biol.* **17**, 30-40. doi:10.1038/nrm.2015.6

De Smet, I., Signora, L., Beeckman, T., Inze, D., Foyer, C. H. and Zhang, H. (2003). An abscisic acid-sensitive checkpoint in lateral root development of Arabidopsis. *Plant J.* **33**, 543-555. doi:10.1046/j.1365-313X.2003.01652.x

Duan, L., Dietrich, D., Ng, C. H., Chan, P. M. Y., Bhalerao, R., Bennett, M. J. and Dinneny, J. R. (2013). Endodermal ABA signaling promotes lateral root

quiescence during salt stress in Arabidopsis seedlings. *Plant Cell* **25**, 324-341. doi:10.1105/tpc.112.107227

Efroni, I., Mello, A., Nawy, T., Ip, P.-L., Rahni, R., DelRose, N., Powers, A., Satija, R. and Birnbaum, K. D. (2016). Root regeneration triggers an embryo-like sequence guided by hormonal interactions. *Cell* **165**, 1721-1733. doi:10.1016/j.cell.2016.04.046

French, A. P., Wilson, M. H., Kenobi, K., Dietrich, D., Voss, U., Ubeda-Tomas, S., Pridmore, T. P. and Wells, D. M. (2012). Identifying biological landmarks using a novel cell measuring image analysis tool: Cell-o-Tape. *Plant Methods* **8**, 7. doi:10.1186/1746-4811-8-7

Fujii, H., Chinnusamy, V., Rodrigues, A., Rubio, S., Antoni, R., Park, S.-Y., Cutler, S. R., Sheen, J., Rodriguez, P. L. and Zhu, J. K. (2009). In vitro reconstitution of an abscisic acid signalling pathway. *Nature* **462**, 660-664. doi:10.1038/nature08599

Geng, Y., Wu, R., Wee, C. W., Xie, F., Wei, X., Chan, P. M. Y., Tham, C., Duan, L. and Dinneny, J. R. (2013). A spatio-temporal understanding of growth regulation during the salt stress response in Arabidopsis. *Plant Cell* **25**, 2132-2154. doi:10.1105/tpc.113.112896

Goh, T., Toyokura, K., Wells, D. M., Swarup, K., Yamamoto, M., Mimura, T., Weijers, D., Fukaki, H., Laplaze, L., Bennett, M. J. et al. (2016). Quiescent center initiation in the Arabidopsis lateral root primordia is dependent on the SCARECROW transcription factor. *Development* **143**, 3363-3371. doi:10.1242/dev.135319

González-Guzmán, M., Apostolova, N., Bellés, J. M., Barrero, J. M., Piqueras, P., Ponce, M. R., Micol, J. L., Serrano, R. and Rodriguez, P. L. (2002). The short-chain alcohol dehydrogenase ABA2 catalyzes the conversion of xanthoxin to abscisic aldehyde. *Plant Cell* **14**, 1833-1846. doi:10.1105/tpc.002477

Hardtke, C. S. and Berleth, T. (1998). The Arabidopsis gene MONOPTEROS encodes a transcription factor mediating embryo axis formation and vascular development. *EMBO J.* **17**, 1405-1411. doi:10.1093/emboj/17.5.1405

Harris, J. M. (2015). Abscisic acid: hidden architect of root system structure. *Plants* **4**, 548-572. doi:10.3390/plants4030548

Hawker, N. P. and Bowman, J. L. (2004). Roles for Class III HD-Zip and KANADI genes in Arabidopsis root development. *Plant Physiol.* **135**, 2261-2270. doi:10.1104/pp.104.040196

Hayashi, K., Tan, X., Zheng, N., Hatate, T., Kimura, Y., Kepinski, S. and Nozaki, H. (2008). Small-molecule agonists and antagonists of F-box protein-substrate interactions in auxin perception and signaling. *Proc. Natl. Acad. Sci. USA* **105**, 5632-5637. doi:10.1073/pnas.0711146105

He, J., Duan, Y., Hua, D., Fan, G., Wang, L., Liu, Y., Chen, Z., Han, L., Qu, L.-J. and Gong, Z. (2012). DEXH box RNA helicase-mediated mitochondrial reactive oxygen species production in Arabidopsis mediates crosstalk between abscisic acid and auxin signaling. *Plant Cell* **24**, 1815-1833. doi:10.1105/tpc.112.098707

Iyer-Pascuzzi, A. S., Jackson, T., Cui, H., Petricka, J. J., Busch, W., Tsukagoshi, H. and Benfey, P. N. (2011). Cell identity regulators link development and stress responses in the Arabidopsis root. *Dev. Cell* **21**, 770-782. doi:10.1016/j.devcel.2011.09.009

Kubo, M., Udagawa, M., Nishikubo, N., Horiguchi, G., Yamaguchi, M., Ito, J., Mimura, T., Fukuda, H. and Demura, T. (2005). Transcription switches for protoxylem and metaxylem vessel formation. *Genes Dev.* **19**, 1855-1860. doi:10.1101/gad.1331305

Kurihara, D., Mizuta, Y., Sato, Y. and Higashiyama, T. (2015). ClearSee: a rapid optical clearing reagent for whole-plant fluorescence imaging. *Development* **142**, 4168-4179. doi:10.1242/dev.127613

Lee, J.-Y., Colinas, J., Wang, J. Y., Mace, D., Ohler, U. and Benfey, P. N. (2006). Transcriptional and posttranscriptional regulation of transcription factor expression in Arabidopsis roots. *Proc. Natl. Acad. Sci. USA* **103**, 6055-6060. doi:10.1073/pnas.0510607103

Leung, J., Bouvier-Durand, M., Morris, P. C., Guerrier, D., Chefdor, F. and Giraudat, J. (1994). Arabidopsis ABA response gene ABI1: features of a calcium-modulated protein phosphatase. *Science* **264**, 1448-1452. doi:10.1126/science.7910981

Li, H., Tiwari, S. B., Hagen, G. and Guilfoyle, T. J. (2011). Identical amino acid substitutions in the repression domain of auxin/indole-3-acetic acid proteins have contrasting effects on auxin signaling. *Plant Physiol.* **155**, 1252-1263. doi:10.1104/pp.110.171322

Liu, Q., Yao, X., Pi, L., Wang, H., Cui, X. and Huang, H. (2009). The ARGONAUTE10 gene modulates shoot apical meristem maintenance and establishment of leaf polarity by repressing miR165/166 in Arabidopsis. *Plant J.* **58**, 27-40. doi:10.1111/j.1365-313X.2008.03757.x

Ma, Y., Szostkiewicz, I., Korte, A., Moes, D., Yang, Y., Christmann, A. and Grill, E. (2009). Regulators of PP2C phosphatase activity function as abscisic acid sensors. *Science* **324**, 1064-1068. doi:10.1126/science.1172408

Mahonen, A. P., Bishopp, A., Higuchi, M., Nieminen, K. M., Kinoshita, K., Tormakangas, K., Ikeda, Y., Oka, A., Kakimoto, T. and Helariutta, Y. (2006). Cytokinin signaling and its inhibitor AHP6 regulate cell fate during vascular development. *Science* **311**, 94-98. doi:10.1126/science.1118875

Malamy, J. E. and Benfey, P. N. (1997). Organization and cell differentiation in lateral roots of Arabidopsis thaliana. *Development* **124**, 33-44.

McConnell, J. R., Emery, J., Eshed, Y., Bao, N., Bowman, J. and Barton, M. K. (2001). Role of PHABULOSA and PHAVOLUTA in determining radial patterning in shoots. *Nature* **411**, 709-713. doi:10.1038/35079635

Miyashima, S., Koi, S., Hashimoto, T. and Nakajima, K. (2011). Non-cell-autonomous microRNA165 acts in a dose-dependent manner to regulate multiple differentiation status in the Arabidopsis root. *Development* **138**, 2303-2313. doi:10.1242/dev.060491

Müller, C. J., Valdés, A. E., Wang, G., Ramachandran, P., Beste, L., Uddenberg, D. and Carlsbecker, A. (2016). PHABULOSA mediates an auxin signaling loop to regulate vascular patterning in arabidopsis. *Plant Physiol.* **170**, 956-970. doi:10.1104/pp.15.01204

Muraro, D., Mellor, N., Pound, M. P., Help, H., Lucas, M., Chopard, J., Byrne, H. M., Godin, C., Hodgman, T. C., King, J. R. et al. (2014). Integration of hormonal signaling networks and mobile microRNAs is required for vascular patterning in Arabidopsis roots. *Proc. Natl. Acad. Sci. USA* **111**, 857-862. doi:10.1073/pnas.1221766111

Naseer, S., Lee, Y., Lapierre, C., Franke, R., Nawrath, C. and Geldner, N. (2012). Casparian strip diffusion barrier in Arabidopsis is made of a lignin polymer without suberin. *Proc. Natl. Acad. Sci. USA* **109**, 10101-10106. doi:10.1073/pnas.1205726109

Orman-Ligeza, B., Morris, E. C., Parizot, B., Lavigne, T., Babe, A., Ligeza, A., Klein, S., Sturrock, C., Xuan, W., Novak, O. et al. (2018). The xerobranching response represses lateral root formation when roots are not in contact with water. *Curr. Biol.* **28**, 3165-3173.e3165. doi:10.1016/j.cub.2018.07.074

Park, S.-Y., Fung, P., Nishimura, N., Jensen, D. R., Fujii, H., Zhao, Y., Lumba, S., Santiago, J., Rodrigues, A., Chow, T. F. et al. (2009). Abscisic acid inhibits type 2C protein phosphatases via the PYR/PYL family of START proteins. *Science* **324**, 1068-1071. doi:10.1016/j.cub.2018.07.074

Park, S.-Y., Peterson, F. C., Mosquna, A., Yao, J., Volkman, B. F. and Cutler, S. R. (2015). Agrochemical control of plant water use using engineered abscisic acid receptors. *Nature* **520**, 545-548. doi:10.1038/nature14123

Parry, G., Calderon-Villalobos, L. I., Prigge, M., Peret, B., Dharmasiri, S., Itoh, H., Lechner, E., Gray, W. M., Bennett, M. and Estelle, M. (2009). Complex regulation of the TIR1/AFB family of auxin receptors. *Proc. Natl. Acad. Sci. USA* **106**, 22540-22545. doi:10.1073/pnas.0911967106

Prigge, M. J., Otsuga, D., Alonso, J. M., Ecker, J. R., Drews, G. N. and Clark, S. E. (2005). Class III homeodomain-leucine zipper gene family members have overlapping, antagonistic, and distinct roles in Arabidopsis development. *Plant Cell* **17**, 61-76. doi:10.1105/tpc.104.026161

Prigge, M. J., Greenham, K., Zhang, Y., Santner, A., Castillejo, C., Mutka, A. M., O'Malley, R. C., Ecker, J. R., Kunkel, B. N. and Estelle, M. (2016). The arabidopsis auxin receptor F-box proteins AFB4 and AFB5 are required for response to the synthetic auxin picloram. *G3 (Bethesda)* **6**, 1383-1390. doi:10.1534/g3.115.025585

Qin, X. and Zeevaart, J. A. D. (1999). The 9-cis-epoxycarotenoid cleavage reaction is the key regulatory step of abscisic acid biosynthesis in water-stressed bean. *Proc. Natl. Acad. Sci. USA* **96**, 15354-15361. doi:10.1073/pnas.96.26.15354

Ramachandran, P., Wang, G., Augstein, F., de Vries, J. and Carlsbecker, A. (2018). Continuous root xylem formation and vascular acclimation to water deficit involves endodermal ABA signalling via miR165. *Development* **145**, dev159202. doi:10.1242/dev.159202

Roppolo, D., De Rybel, B., Dénervaud Tendon, V., Pfister, A., Alassimone, J., Vermeer, J. E. M., Yamazaki, M., Stierhof, Y. D., Beeckman, T. and Geldner, N. (2011). A novel protein family mediates Casparian strip formation in the endodermis. *Nature* **473**, 380-383. doi:10.1038/nature10070

Schachtman, D. P. and Goodger, J. Q. D. (2008). Chemical root to shoot signaling under drought. *Trends Plant Sci.* **13**, 281-287. doi:10.1016/j.tplants.2008.04.003

Sebastian, J., Ryu, K. H., Zhou, J., Tarkowská, D., Tarkowski, P., Cho, Y.-H., Yoo, S.-D., Kim, E.-S. and Lee, J.-Y. (2015). PHABULOSA controls the quiescent center-independent root meristem activities in Arabidopsis thaliana. *PLoS Genet.* **11**, e1004973. doi:10.1371/journal.pgen.1004973

Sena, G., Wang, X., Liu, H.-Y., Hofhuis, H. and Birnbaum, K. D. (2009). Organ regeneration does not require a functional stem cell niche in plants. *Nature* **457**, 1150-1153. doi:10.1038/nature07597

Shani, E., Salehin, M., Zhang, Y., Sanchez, S. E., Doherty, C., Wang, R., Mangado, C. C., Song, L., Tal, I., Pisanty, O. et al. (2017). Plant stress tolerance requires auxin-sensitive Aux/IAA transcriptional repressors. *Curr. Biol.* **27**, 437-444. doi:10.1016/j.cub.2016.12.016

Taylor-Teeples, M., Lin, L., de Lucas, M., Turco, G., Toal, T. W., Gaudinier, A., Young, N. F., Trabucco, G. M., Veling, M. T., Lamothe, R. et al. (2015). An Arabidopsis gene regulatory network for secondary cell wall synthesis. *Nature* **517**, 571-575. doi:10.1038/nature14099

Tucker, M. R., Hinze, A., Tucker, E. J., Takada, S., Jurgens, G. and Laux, T. (2008). Vascular signalling mediated by ZWILLE potentiates WUSCHEL function during shoot meristem stem cell development in the Arabidopsis embryo. *Development* **135**, 2839-2843. doi:10.1242/dev.023648

Ursache, R., Miyashima, S., Chen, Q., Vaten, A., Nakajima, K., Carlsbecker, A., Zhao, Y., Helariutta, Y. and Dettmer, J. (2014). Tryptophan-dependent auxin biosynthesis is required for HD-ZIP III-mediated xylem patterning. *Development* **141**, 1250-1259. doi:10.1242/dev.103473

Verslues, P. E., Agarwal, M., Katiyar-Agarwal, S., Zhu, J. and Zhu, J. K. (2006). Methods and concepts in quantifying resistance to drought, salt and freezing,

abiotic stresses that affect plant water status. *Plant J.* **45**, 523-–539. doi:10.1111/j.1365-313X.2005.02593.x

Xing, L., Zhao, Y., Gao, J., Xiang, C. and Zhu, J.-K. (2016). The ABA receptor PYL9 together with PYL8 plays an important role in regulating lateral root growth. *Sci. Rep.* **6**, 27177. doi:10.1038/srep27177

Yu, Y., Ji, L., Le, B. H., Zhai, J., Chen, J., Luscher, E., Gao, L., Liu, C., Cao, X., Mo, B. et al. (2017). ARGONAUTE10 promotes the degradation of miR165/6 through the SDN1 and SDN2 exonucleases in Arabidopsis. *PLoS Biol.* **15**, e2001272. doi:10.1371/journal.pbio.2001272

Zhang, H., Han, W., De Smet, I., Talboys, P., Loya, R., Hassan, A., Rong, H., Jurgens, G., Paul Knox, J. and Wang, M.-H. (2010). ABA promotes quiescence of the quiescent centre and suppresses stem cell differentiation in the Arabidopsis primary root meristem. *Plant J.* **64**, 764-774. doi:10.1111/j.1365-313X.2010.04367.x

Zhao, Y., Xing, L., Wang, X., Hou, Y.-J., Gao, J., Wang, P., Duan, C.-G., Zhu, X. and Zhu, J.-K. (2014). The ABA receptor PYL8 promotes lateral root growth by enhancing MYB77-dependent transcription of auxin-responsive genes. *Sci. Signal.* **7**, ra53. doi:10.1126/scisignal.2005051

Zhu, H., Hu, F., Wang, R., Zhou, X., Sze, S.-H., Liou, L. W., Barefoot, A., Dickman, M. and Zhang, X. (2011). Arabidopsis Argonaute10 specifically sequesters miR166/165 to regulate shoot apical meristem development. *Cell* **145**, 242-256. doi:10.1016/j.cell.2011.03.024

Supplementary Materials and Methods

Plant materials

The *abi1-1* (Leung et al., 1994), *pyr1;pyl1;pyl2;pyl4* (Park et al., 2009), *aba2-1* (Gonzalez-Guzman et al., 2002), *tir1-1;afb2-3;afb4-8;afb5-5* (NASC, (Prigge et al., 2016)), *scr3* (Fukaki et al., 1998), *shr2* (Helariutta et al., 2000). *p35S::PYR1^{MANDI}* (Park et al., 2015), *pSCR::abi1-1/pUAS::abi1-1* (Duan et al., 2013), *35S::Iaa6m1m2* (Li et al., 2011), *pS18::ER-GFP* (Lee et al., 2006), *pVND7::YFP-NLS* (Kubo et al., 2005), *pAHP6::GFP-ER* (Bishopp et al., 2011), *pMIR165a::GFP/pMIR166b::GFP* (Carlsbecker et al., 2010), *pPHB::PHB-GFP/pPHB::GFP-ER* (Miyashima et al., 2011), *DR5::Venus-NLS* (Heisler et al., 2005), *DII-Venus* (Brunoud et al., 2012), and *zll/pZLL::YFP:ZLL* (Tucker et al., 2008) are in *Col-0*. The *phb-13;phv-11;cna-2* (Prigge et al., 2005) is in the *Col (er2)* and *phb-1d* (McConnell et al., 2001) is in the *Ler*. For tissue-specific expression various enhancer trap lines were crossed to plants harboring *pUAS::abi1-1*. For control experiments the *C24* background was crossed to *pUAS::abi1-1*. Analyses were done on F1 generation of crosses as previously described (Duan et al., 2013). To evaluate the effect of mandipropamid on *miR165-GFP* expression, homozygous *p35S::PYR1^{MANDI}* and *pMIR165a::GFP* transgenes were crossed and analyzed in F1 progeny.

Growth conditions

Seeds were surface-sterilized by vapor-phase sterilization in a closed container with 6 ml concentrated HCl (32%) added to 100 ml bleach (11%) for 1.5-2 hours and ventilated for 15 min in sterile environment. Seeds were sown on standard plates containing 0.5X Murashige & Skoog (0.5X MS) salt mixture (Sigma M5519) titrated to pH 5.7 with MES and KOH, 1% sucrose, and 0.8% agar and vernalized for 2 days at 4 °C. Plates were transferred to a growth chamber and grown vertically under long-day conditions (16 h light/8 h dark cycles) at 21 °C. The light intensity was 100 $\mu E \cdot m^{-2} \cdot s^{-1}$.

Cell length measurements

Confocal images were acquired with Zeiss Plan-Apochromat 20X/0.8 M27 objective as tile-scan in the middle section of roots. Cell lengths measurements were carried out with semi-automated Cell-o-Tape, ImageJ (Fiji) macro (Band et al., 2012). All measurements were done on the cortex cell layer with numbering starting from the first initial adjacent to the QC. The position of the ETZ for each root was first estimated automatically by the built-in TSZ feature in Cell-o-Tape and then confirmed manually by the requirement that at least three adjacent cells had a minimum of 20% increase in cell length. Size of the elongation zone (e.g., exit to maturation) was calculated on cortex cells starting from ETZ until the position at which the first root hair emerged. In *Col-0* it is usually eight or nine cells.

Confocal microscopy

Images were captured on Zeiss LSM 780-NLO laser-scanning confocal microscope with Plan-Apochromat 20X/0.8 and C-Apochromat 40X/1.20 W Korr FCS objectives (Zeiss). For time-lapse experiments LD Plan-Neofluar 40X/0.6 was used. Emission was detected with GaAsP spectral detector. Imaging settings were as follows: PI, excitation with 561 nm diode laser and emission between 590-650 nm; GFP, excitation with argon laser at 488 nm and emission between 505-545 nm; Venus, excitation with argon laser at 514 nm and emission between 520-560 nm; calcofluor white, excitation with 405 nm diode laser and emission between 420-470 nm; basic fuchsin, excitation with 561 nm diode and emission between 580-640 nm. For simultaneous detection of PI and Venus, spectral separation lambda mode was used with 514 nm argon excitation and emission set between 520-600 nm with 8.9-nm step intervals. In lateral roots high levels of autofluorescence were detected even after clearing, thus for separation of autofluoresence from GFP signal in LRI spectral separation lambda mode was used with 488 nm argon excitation and emission set between 500-550 nm with 8.9-nm step intervals. Image analyses were performed with Fiji and Zeiss ZEN10.

Gene expression by quantitative RT-PCR

For analysis of gene expression *Col-0*, *abi1-1*, and *pyr1;pyl1;pyl2;pyl4* 5-DAG seedlings were treated with 10 µM ABA or 0.1% ethanol liquid solution in 0.5X MS for 1 h. *p35S::PYR1*^{MANDI} 5-DAG seedlings were treated with 10 µM mandipropamid or 0.1% methanol for 3 h. For 24-h treatments *Col-0* 5-DAG seedlings were transferred to plates supplemented with 10 µM ABA or 0.1% ethanol. Tissue was collected from 60-70 roots for each genotype and treatment. The first 0.5 cm of root (close to root tip) was dissected under a dissecting microscope and used for RNA extraction. Total RNA was extracted with miRNeasy Micro Kit (Qiagen, 217084) and treated with DNase (Qiagen, 79254) to eliminate possible DNA contamination. Total RNA (0.5 µg per sample) was used for reverse transcription with High Capacity cDNA Reverse Transcription Kit (Applied Biosystems, 4368814). For quantitative RT-PCR, Fast SYBR Green Master Mix (Applied Biosystems, 4385612) was used in 15-µl reactions. Cycles were run on Applied Biosystems StepOnePlus PCR system. Three-stage PCR reactions were done with three technical replicates and annealing at 60 °C. *PP2A* (*At1G13320*) expression is stable under ABA treatments and was used as a reference for normalization of the data. At least three biological replicates were done for each genotype and treatment, and representative experiments are presented in figures.

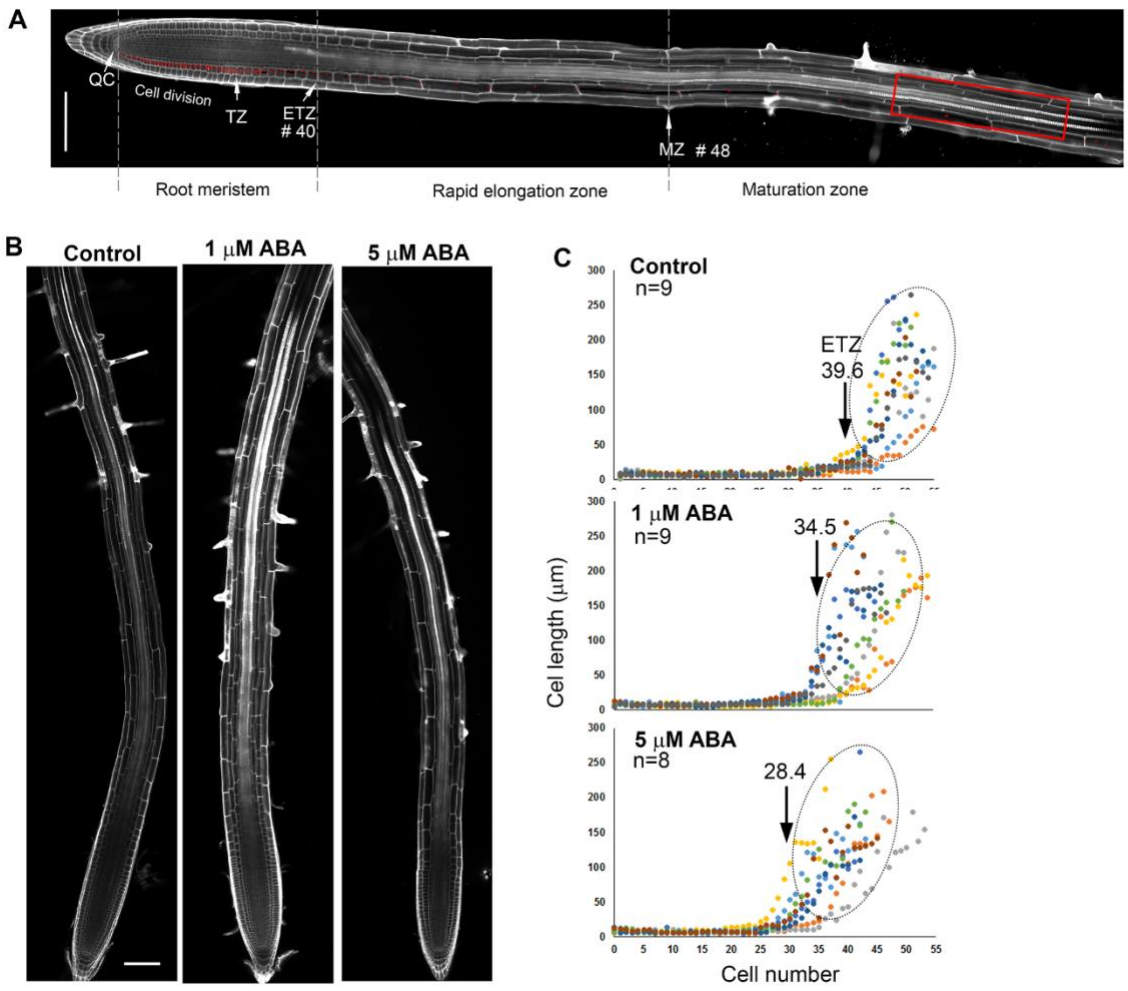

Fig. S1. **Response of the primary root to ABA.** *(A)* A tile scan image of a *Col-0* WT primary root stained with PI. Cortex cell numbers marked in red. Meristematic zone includes dividing and transiently amplifying (transition zone) cells, around 40 cells in WT. The end of the transition zone (ETZ) defines the beginning of rapid cell elongation zone. The position of root hair emergence relative to ETZ defines the size the elongation zone (8-9 cells in WT) and characterizes the rate of root maturation/differentiation. QC, quiescence center; TZ, start of the transition zone; ETZ, end of transition zone; MZ, initiation of the maturation zone determined by the appearance of root hair cells. Red rectangle marks the region where morphology of vascular tissues was analyzed: 3-4 cells distal to the first root hair cell or 11-13 cells from the ETZ. (*B*) Primary roots following 24-h treatment with the indicated concentrations of ABA. EtOH treatment served as a control. Cell walls were stained with PI. (*C*) Cell length analysis, starting from QC, following 24-h treatment with ABA. Independent roots (n) are presented in different colors. Numbers and arrows mark the average positions of the ETZ. Note the response of roots to ABA with regard to meristem size (position of ETZ) and cell length distributions at the elongation/maturation zone (ellipses). Scale bars in panels *A* and *B*, 100 μm.

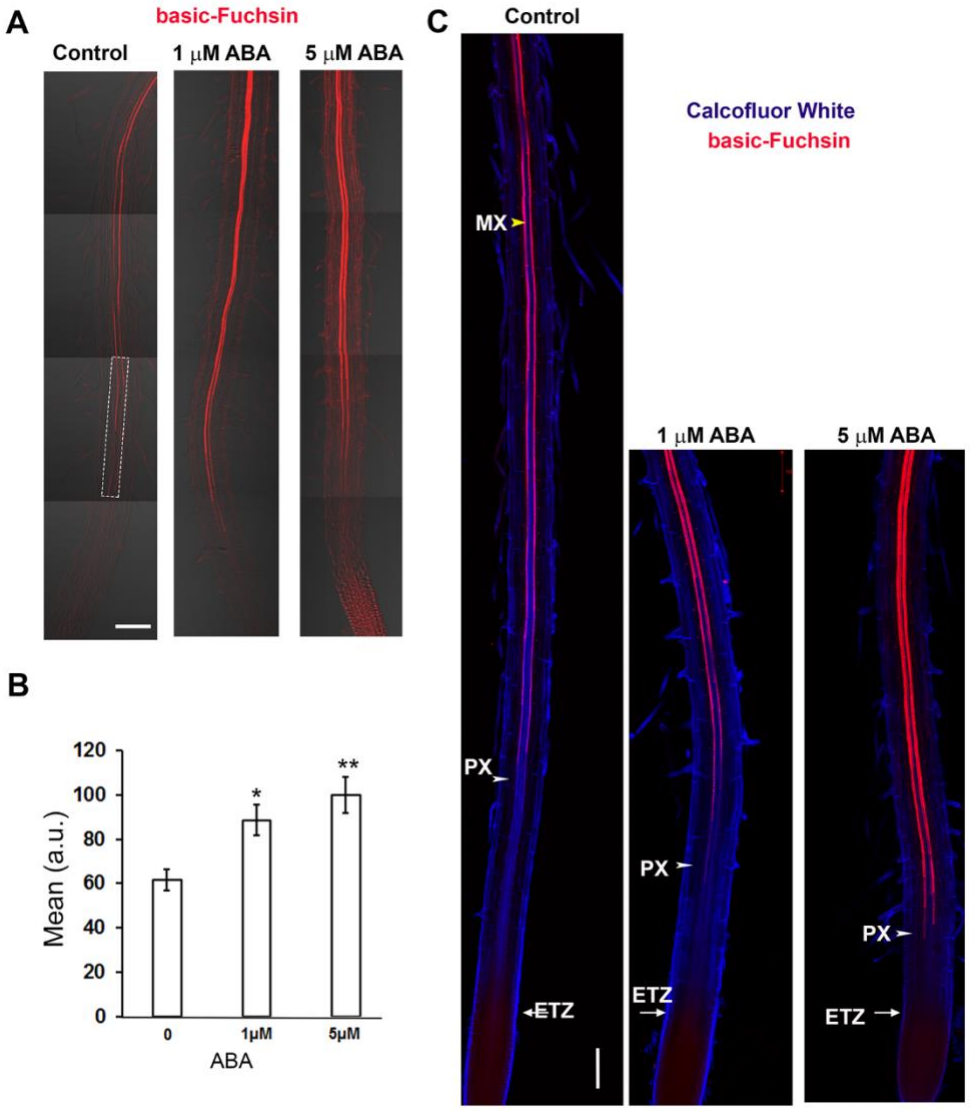

Fig. S2. **Effect of ABA on xylem lignification.** (*A*) Tile images of *Col-0* roots stained with basic-fuchsin (red) following 24-h incubation in control or ABA-containing media. The white rectangle defines the region where measurements were performed. Scale bar, 100 µm. (*B*) Bar graph presenting the mean fluorescent intensity of fuchsin in vascular tissue of the maturation zone (n = 6 per treatment). Error bars are SE. Statistically significant differences (*p≤ 0.05; ** p≤ 0.005) relative to controls were computed based on the Student's t-tests, two-tail distribution, unequal variance. (*C*) Double staining of primary cell walls of cleared *Col-0* roots with calcofluor white (blue) and lignified SCW with basic-fuchsin (red). Note the difference between position of PX and MX differentiation at control conditions and earlier lignification of PX after ABA treatments. Scale bar, 100 µm.

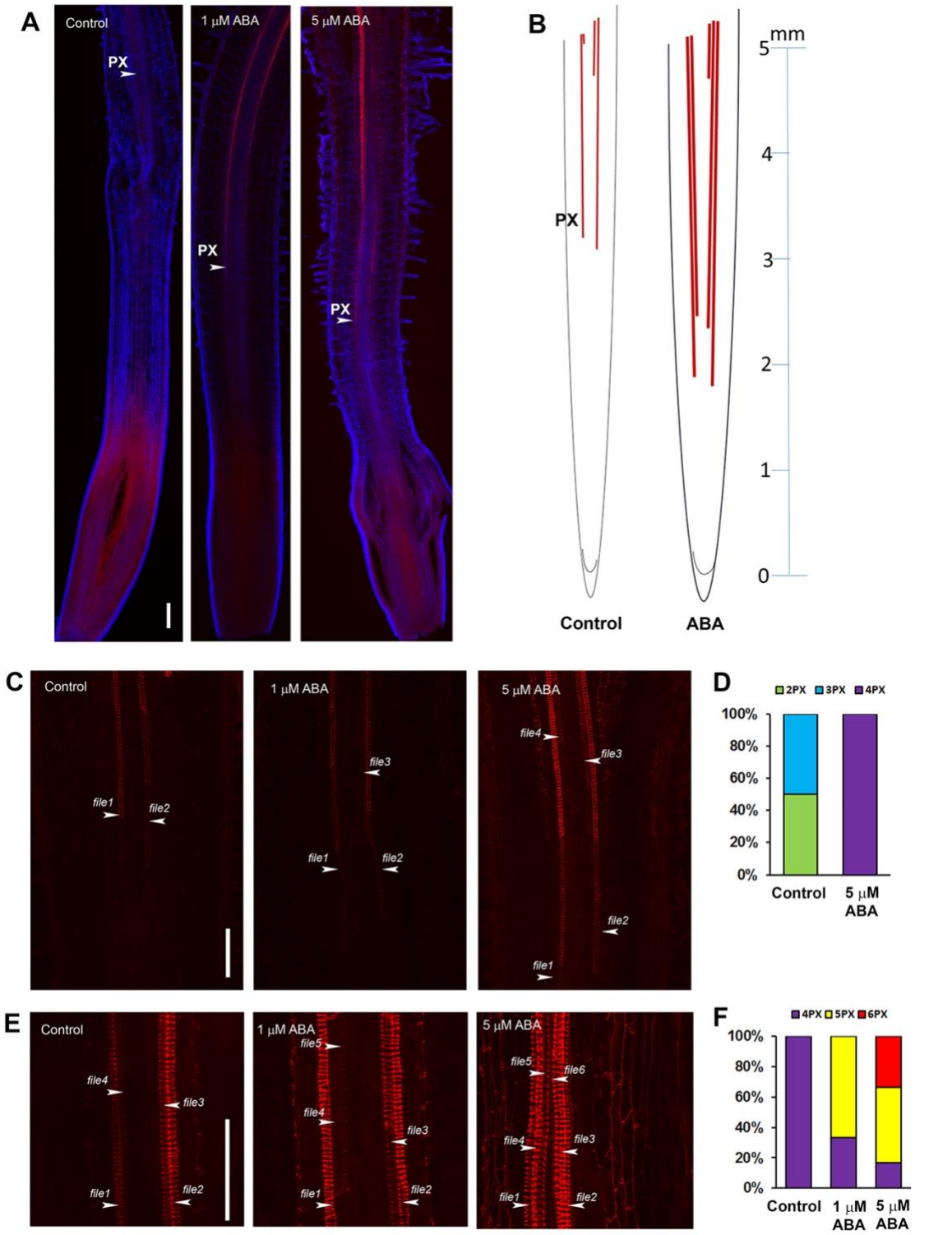

Fig. S3. **Effects of ABA on PX differentiation in tomato.** (*A*) Tomato (*Solanum lycopersicum* M82) roots treated with ethanol (control) or with ABA at indicated concentrations for 48 hours, cleared and stained with calcofluor white (blue) and basic-fuchsin (red). The position of PX is defined. *(B)* A scheme displaying the effect of ABA treatments on PX differentiation. Note that tomato roots have 4 PX cell files two of which differentiate 2-3

mm from the tip and the second pair about 5 mm from the tip. ABA induces earlier differentiation of all 4 PX files and formation of additional PX files about 5 mm form the tip. *(C)* Close-up view of first lignified PX cell files in differentiation region of *M82* tomato root. Lignified PX cell files are indicated with white arrowheads. Images are Z-stack maximal projections. *(D)* Frequencies of PX cell file numbers in differentiation region of the root in control or ABA treated conditions (n=4 in control, n=5 in 5 µM ABA). *(E)* Close-up view of PX in the mature root region at distance of around 5 mm form root tip. Lignified PX cell files are indicated with white arrowheads. Images are Z-stack maximal projections. *(F)* Frequencies of PX cell file numbers in mature region of root in control or ABA treated conditions (n=4 in control, n=6 in 1 µm and 5 µM ABA). Scale bars in panels *A*, *C* and *E*, 100 µm.

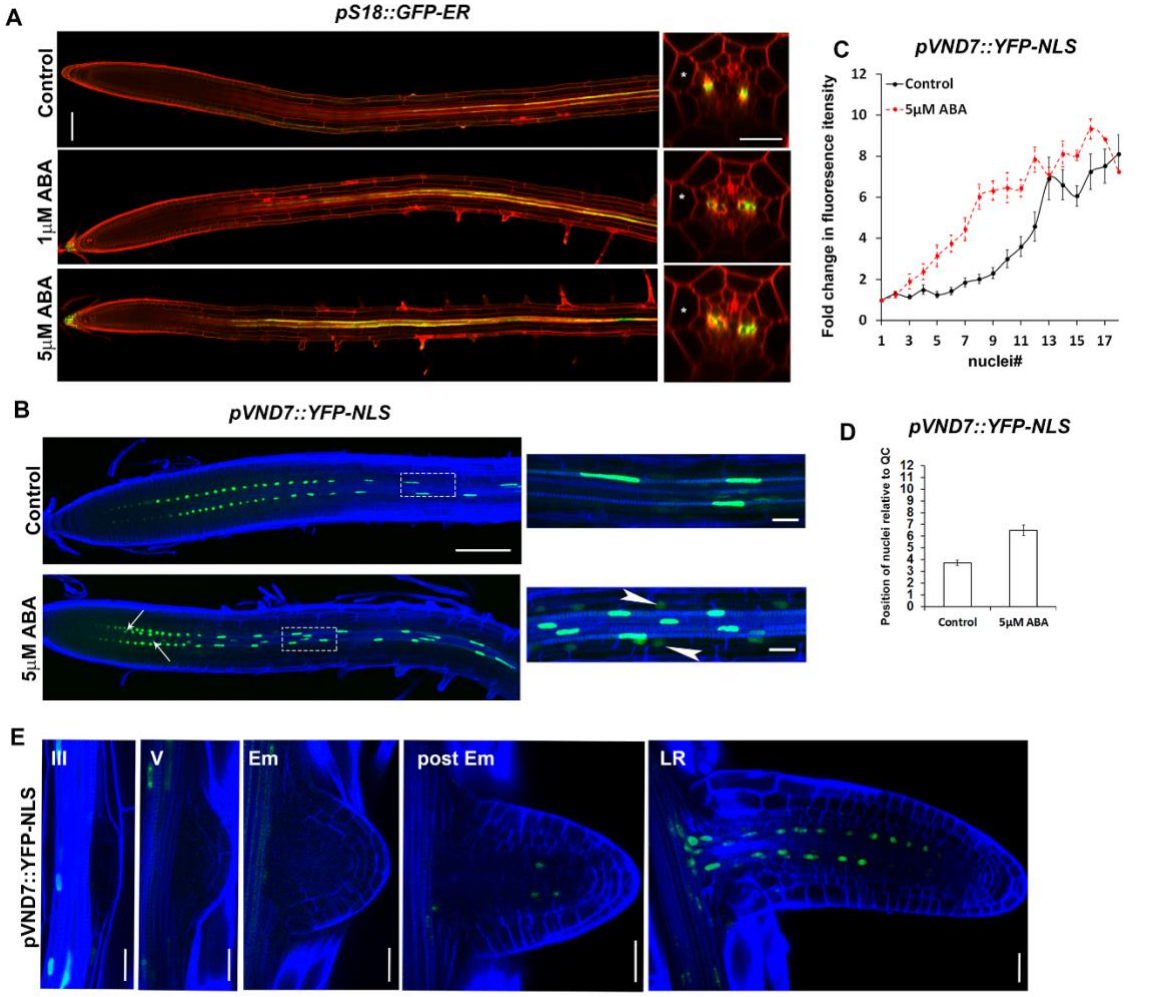

Fig. S4. **Effect of ABA on expression of PX differentiation markers.** *(A)* Expression of the maturing PX marker *pS18::ER-GFP* (green) following 24-h treatment with ABA or with EtOH as a control. Cell walls were stained with PI (red). Asterisks indicate endodermis. *(B)* Expression of *pVND7::YFP-NLS* (green) in cleared roots stained with calcofluor white (blue) after treatment with 5 µM ABA or with EtOH as a control. Arrows indicate additional cell files of xylem cells expressing YFP-NLS. Rectangles mark regions in the elongation zone enlarged at the right. Arrowheads indicate spreading of VND7 expression to pericycle after ABA treatment. *(C)* Mean fold change in YFP-NLS nuclear signal intensity relative to the expression levels in the first nucleus. Values on x-axis are nuclei numbers starting from the first nuclei with expression. Note that ABA treatments induce fast increase in *pVND7::YFP-NLS* expression levels compared to control treatments were VND7 expression increased gradually in the first nine nuclei. (n= 18 cell files per treatment). *(D)* Position of the first *pVND7::YFP-NLS* positive nuclei in PX provascular cells relative to QC after ABA and EtOH (Control) treatments (n=18 cell files per treatment). (*E*) pVND7::YFP-NLS expression in lateral roots. Stages of development are indicated. Em – emergence. Scale bars 100 µm in panel *A* left images and 20 µm for Z-stacks at the right, 100 µm in panel *B* left images and 10 µm in magnifications on the right and 20 µm in E. Error bars, SE.

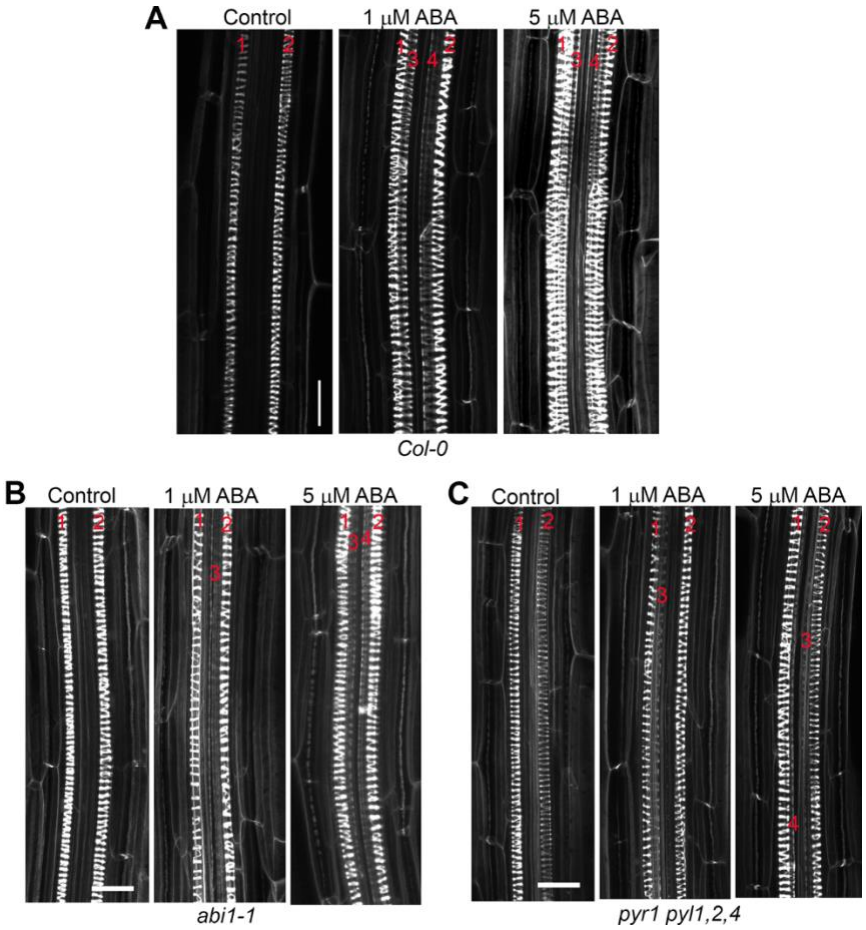

Fig. S5. **Formation of extra PX cell files is suppressed in ABA signaling mutants.** Z-stack maximal projections of roots in (*A*) WT, (*B*) *abi1-1*, and (*C*) *pyr1;pyl1;pyl2;pyl4* mutant seedlings treated with ABA. Note that additional files of PX (red digits) in *abi1-1* and *pyr1;pyl1;pyl2;pyl4* mutants treated with ABA have less defined and weakly stained spiral SCW patterns. Cell walls were stained with PI (white). Scale bars, 20 μm.

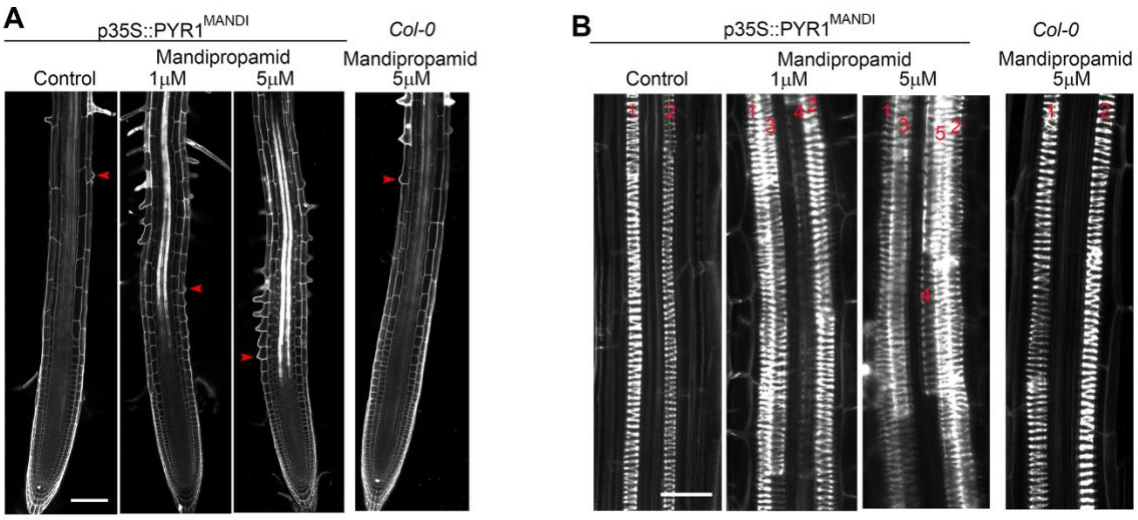

Fig. S6. **Mandipropamid treatment of *p35S:PYR1^{MANDI}* seedlings induces formation of extra PX.** *(A)* Roots of *p35S:PYR1^{MANDI}* and *Col-0* (WT) plants treated with mandipropamid for 24 h. Red arrowheads mark the position of the first emerging root hairs. Scale bar, 100 µm. *(B)* Z-stack maximal projections of roots of *p35S:PYR1^{MANDI}* and *Col-0* seedlings treated with 1 or 5 µM mandipropamid. Mandipropamid induced differentiation of four or five PX files (red digits), respectively, in *p35S:PYR1^{MANDI}* but not in WT control roots. Scale bar, 20 µm. Cell walls were stained with PI (white).

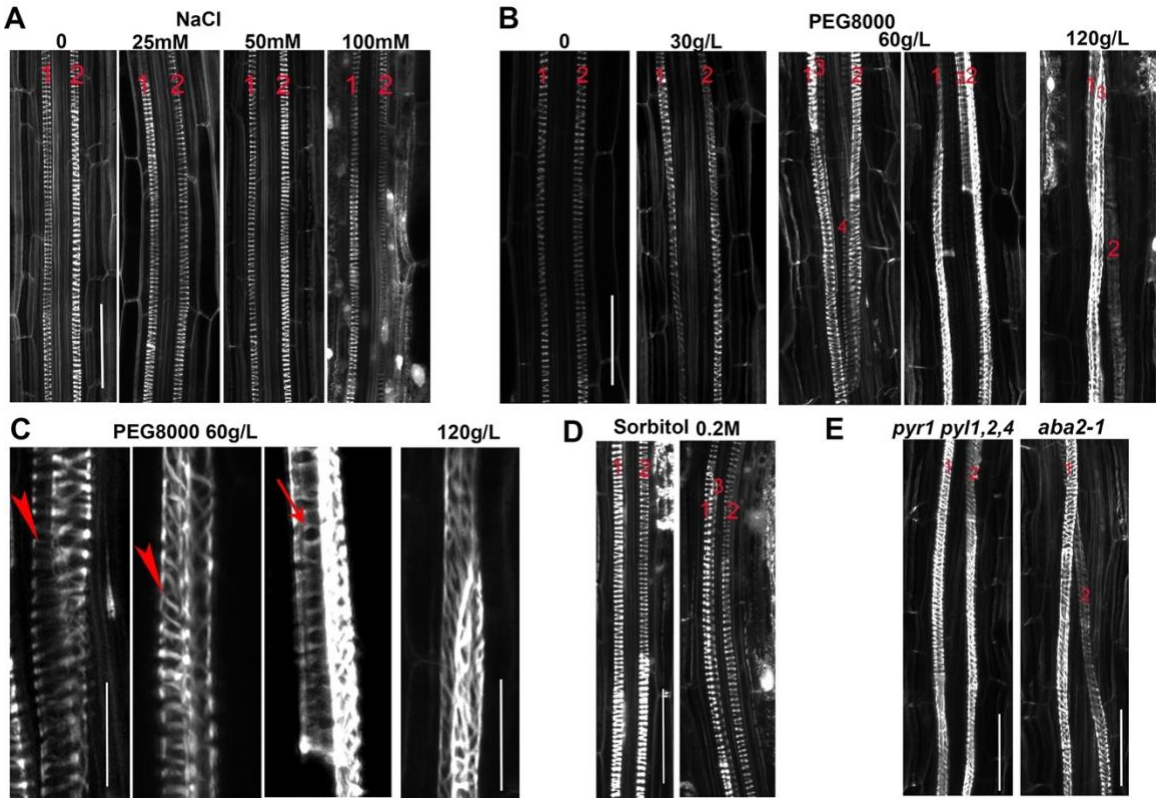

Fig. S7. **Effect of salt and osmotic stress on xylem development in WT and ABA mutants.** *(A)* Xylem architecture after 24-h treatments with the indicated concentrations of NaCl. Only two PX files are observed at all concentrations. *(B)* Xylem structure 24 h after treatments with the indicated concentrations of PEG 8000. Additional PX files were detected following treatments with 60 g/L and 120 g/L. *(C)* Close-up view of *Col-0* xylem cells treated with PEG 8000. The secondary cell wall patterns in xylem are disorganized with some similar to PX (arrowheads); others form atypical MX (arrow). Note the strong effect on secondary cell wall patterning in the 120 g/L PEG 8000-treated roots. *(D)* Xylem structure after 24-h treatments with 0.2 M sorbitol. Additional PX files are observed. *(E)* Xylem architecture of *aba2-1* and *pyr1;pyl1;pyl2;pyl4* mutants following treatments with 60g/L PEG-8000. Images show roots that do not form additional PX cell files. All images are Z-stack maximal projections of vascular tissue. Cell walls were stained with PI. Numbers indicate xylem cell files. Scale bars in panels *A*, *B*, *D*, and *E*, 20 µm; in panel *C*, 10 µm.

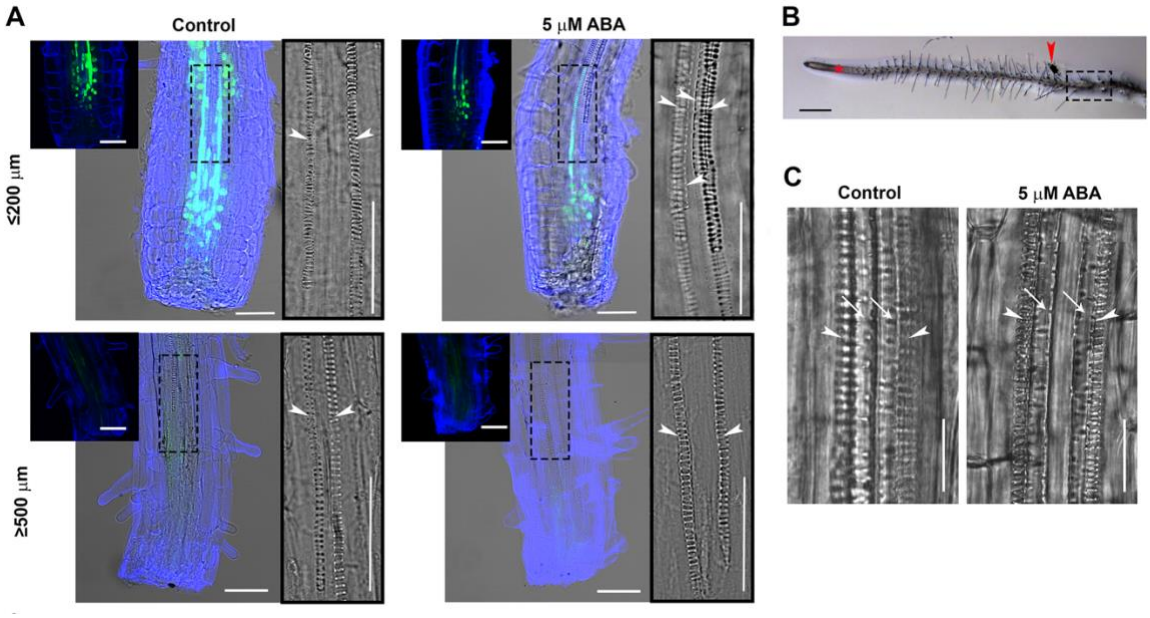

Fig. S8. **Meristem function is required for ABA-induced formation of PX.** Roots were excised at distances ≤200 μm or ≥500 μm from the tip. Alternatively, the roots were labeled at the initiation of the elongation zone. Xylem development was examined after 24 h. Cell walls were stained with calcofluor white (blue). *(A)* DIC images of cleared calcofluor white-stained (blue) *DR5::Venus-NLS* (green) roots following excisions at distances ≤ 200 μm or ≥ 500 μm from the tip and subsequent 24-h treatment with solvent control or 5 μM ABA. Insets, fluorescent images displaying the regenerating auxin maximum (green) in excised tips. Rectangles, regions of enlarged DIC xylem imaging (right). Arrowheads indicate PX. *(B)* Roots were labeled at the initiation of elongation zone (red asterisk indicates the original position of coal relative to root meristem). Red arrowhead marks the position of the label after 24 h. Dashed rectangle highlights the region of enlarged DIC image displayed in panel *C*. *(C)* DIC images displaying xylem differentiation in the region defined by dashed rectangle in panel *B*. Arrowheads indicate PX; arrows, MX. Scale bars in panel *A*, 50 μm; in panel *B*, 500 μm; and in panel *C*, 20 μm.

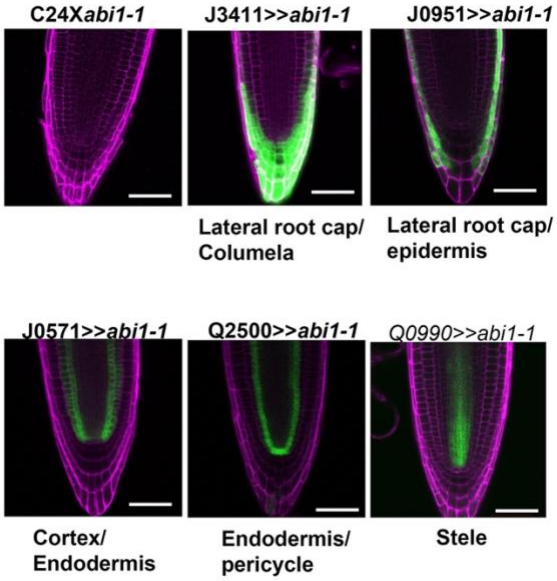

Fig. S9. **Tissue-specific expression of enhancer trap lines crossed to *pUAS::abi1-1*.** (*A*) Confocal images of primary roots of *pUAS::abi1-1* crossed to enhancer trap lines and C24 background, for control, in F1 progeny. Cell walls were stained with PI (magenta). (B) Expression of stele/endodermis and cortex/endodermis-specific *pUAS::abi1-1* lines Q2500 and J0571, respectively in cleared lateral root initials at stage V and emergence (Em). Cell walls were stained with calcofluor white (blue). Activity domain of GAL4 enhancer trap lines was visualized by GFP (green). Scale bars, 50 µm in A and 20 µm B.

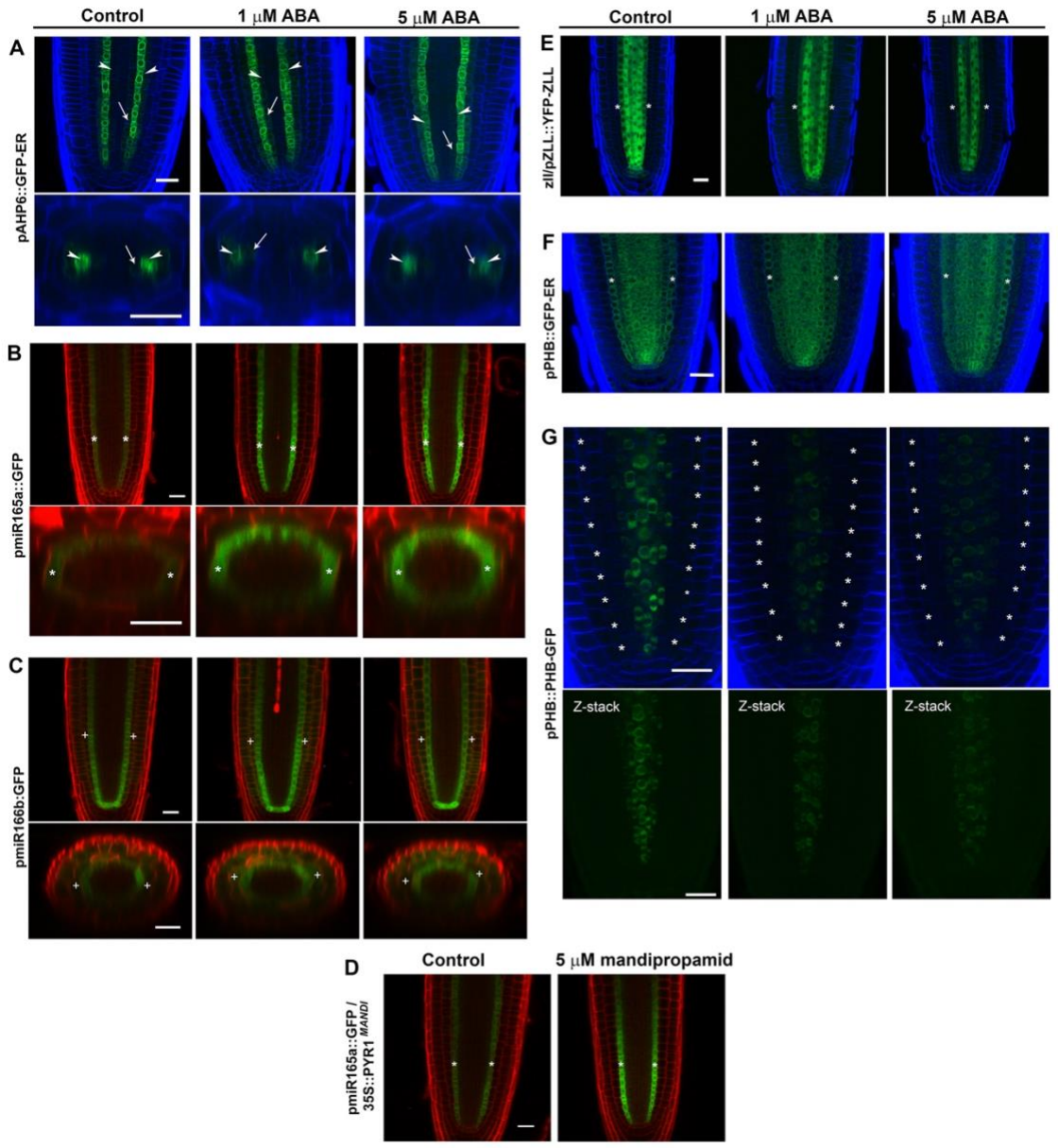

Fig. S10. **ABA alters radial patterning regulators in the meristem.** *(A) pAHP6::GFP-ER* expression (green) in root meristem of cleared roots following 24 h treatments with indicated concentrations of ABA and ethanol for control. Lower panels are Z-cross sections. Note that expression was detected in PX (arrowhead) and at low levels in pericycle and MX (arrow). *(B)* Expression of *pmiR165a::GFP-ER* (green) in root meristem following 24 h treatments with indicated concentrations of ABA and ethanol for control. Asterisks mark the endodermis. Lower panels are Z-cross sections. *(C)* Expression of *pmiR166b::GFP-ER* (green) in root meristem following 24 h treatments with indicated concentrations of ABA and ethanol for control. + indicates cortex. Lower panels are Z-cross sections. *(D)* Expression of *pmiR165a::GFP-ER* (green) in *p35S:PYR1*^{MANDI} background treated with control (ethanol) or 5 μM mandipropamid for 24 h. Asterisks mark

the endodermis. *(E) zll/pZLL::YFP-ZLL* expression (green) in root meristem of cleared roots following 24 h treatments with indicated concentrations of ABA and ethanol for control. Asterisks mark the endodermis. *(F) pPHB::GFP-ER* expression (green) in cleared root meristem following 24 h treatments with indicated concentrations of ABA and ethanol for control. Asterisks mark the endodermis. *(G)* Single scans through the middle of root meristem displaying expression of *pPHB::PHB-GFP* (green) in cleared root tips following 24 h treatments with indicated concentrations of ABA and ethanol for control. Asterisks mark the endodermis. Lower panels Z-stack maximal projections. Note that both PHB-GFP expression levels and the size of expression domain are reduced under ABA treatments. In panels *A*, *E*, *F*, and *G* cell walls in cleared roots were stained with calcofluor white (blue). In panels *B-D*, roots were stained without clearing with PI (red). Fluorescence of GFP/YFP-based reporters is shown in green. Scale bars, 20 μm. In box plots, x indicates the mean, lines indicate the median. Error bars, SE. Statistically significant differences relative to controls (*$p \leq 0.05$; ** $p \leq 0.005$; *** $p \leq 0.0005$) were computed based on the Student's t-tests, two-tail distribution, unequal variance.

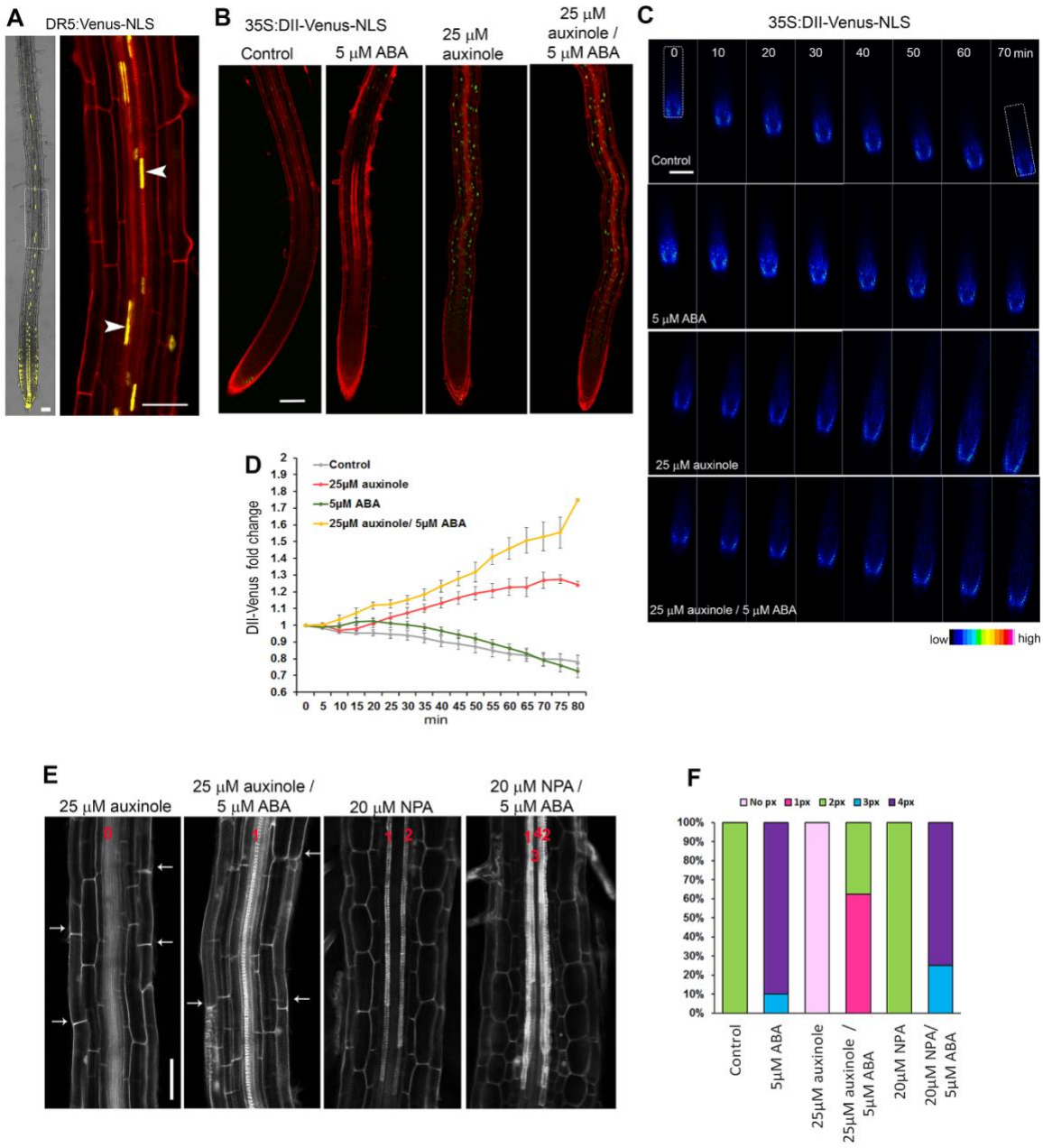

Fig. S11. **ABA induces differentiation of additional PX when auxin signaling or transport are repressed by drug treatments.** *(A)* Expression pattern of DR5::Venus-NLS (yellow). Cell walls were stained with PI (red). Left panel, DIC/fluorescence overlay. The dashed rectangle marks the enlarged region shown to the right. Arrowheads indicate elongated nuclei that are typical of differentiating PX cells. Note that in the maturation zone Venus-NLS expression is primarily detected in the PX. *(B)* The effect of 24-h treatment with indicated agent on the expression of 35S::DII-Venus (green). Cell walls were stained with PI (red). Auxinole treatment resulted in increased DII-Venus fluorescence. *(C)* Time series of representative *35S::DII-Venus* roots following application of ABA and auxinole. DII-Venus fluorescence is represented as a range of intensities.

White rectangles mark regions of root that were used for quantification in panel D. (*D*) Fold change (relative to time 0, which was taken as 1) in DII-Venus fluorescence intensity after application of ABA and auxinole at the indicated concentrations (n=5-6 roots /treatment). (*E*) Vascular tissue composition following 24 h treatments at the indicated concentrations of drugs and hormones. Note induction of PX differentiation by ABA in auxinole treated plants and inhibition of root hair emergence (arrows) with auxinole. (*F*) Frequency of PX formed following the drug and hormone treatments described in panel D (n=8-10/treatment). *S*cale bars in panels *A*, *B* and E, 50 μm and 100 μm in *C*.

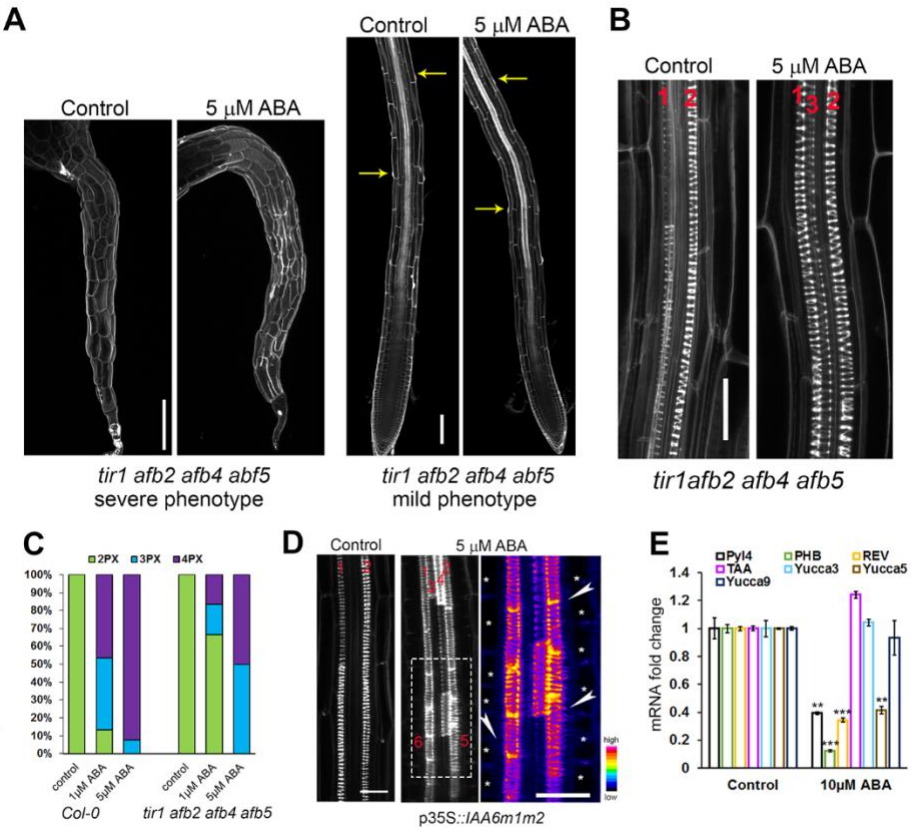

Fig. S12. **ABA response in auxin signaling mutants and effect on expression of auxin biosynthesis genes.** *(A)* Strong and mild phenotype of *tir1;afb2;afb4;afb5* mutant with and without ABA treatment. Note that in mutants with mild phenotype only emerging but not grown root hairs (yellow arrows) are detected, in agreement with compromised auxin signaling in this mutant. (*B*) PX differentiation in *tir1;afb2;afb4;afb5* mutant 24 h following incubation in control or 5 µM ABA media. (*C*) Frequencies of additional PX files formed in *tir1;afb2;afb4;afb5* compared to *Col-0* (*Col-0* n=8-10; *tir1;afb2afb4;afb5* n=9 per treatment). (*D*) PX differentiation in p*35S::IAA6m1m2* treated with 5 µM ABA. The far-right panel is an intensity range zoom of the region defined by the white dashed rectangle. Asterisks indicate endodermis, arrowheads indicate spiral SCW in the pericycle. (*E*) Q-PCR analysis of relative transcript levels in roots of auxin biosynthesis genes (TAA, YUCCA3, YUCCA5 and YUCCA9), *PHB*, *REV* and PYL4 after 3 h treatments with 10 µM ABA. ** p≤ 0.005; *** p ≤ 0.0005 Student's t-tests, two-tail distribution, unequal variance. Scale bars in panel *A*, 100 µm; in *B*, 20 µm; and *D* 50 µm.

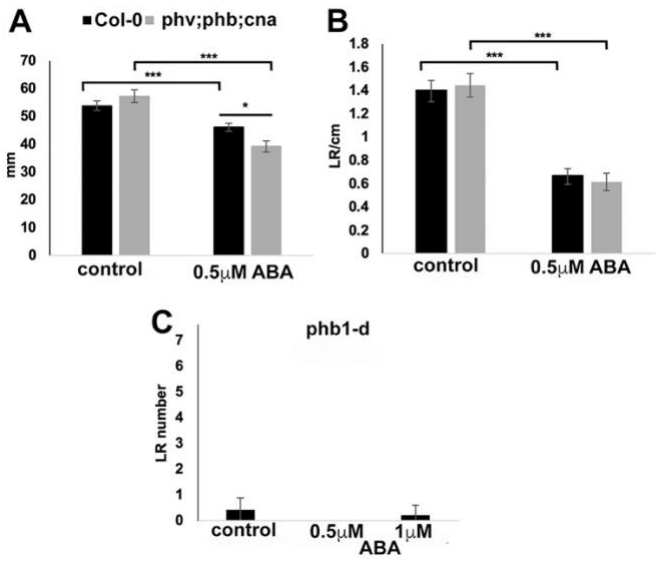

Fig. S13. **The effect of ABA on primary root length and lateral root density and number in triple HD-ZIPIII *phb phv cna* loss of function mutant and miR165/166 resistant *phb1-d* mutant.** A)primary root length of Col-0 and phb phv cna. B) Lateral root (LR) density of Col-0 and *phb phv cna*. C) Lateral root (LR) number in ph1-d. Control (ethanol). *p≤0.05, ***p≤0.0005 Student's t-test.

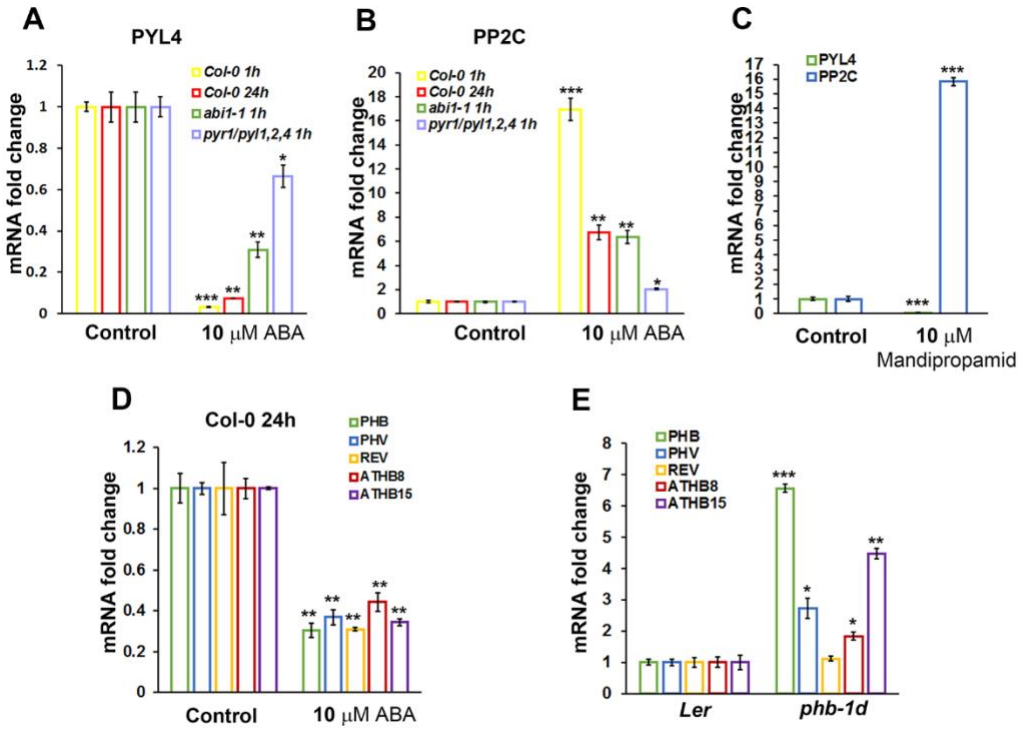

Fig. S14. **Q-PCR analysis of ABA responsive genes *PYL4* and *PP2C* and HD-ZIPIII mRNAs following treatments with ABA or mandipropamid.** (*A-B*) Relative transcript levels of *A*) *PYL4* and *B*) *PP2C* in *Col-0*, *abi1-1*, and *pyr1;pyl1;pyl2;pyl4* after 1 h and *Col-0* after 24-h treatments with 10 µM ABA. Note that after 24 h for *Col-0* or after 1 h for *abi1-1* and *pyr1;pyl1;pyl2;pyl4* the response to ABA of both *PYL4* and *PP2C* decreases compared to that of *Col-0* seedlings treated with ABA for 1 h. (*C*) Relative expression levels of *PYL4* and *PP2C* in *p35S:PYR1*^{MANDI} seedlings after 3 h treatment with 10 µM mandipropamid. (*D*) Relative transcript levels of HD-ZIPIII mRNAs following 24-h treatment with 10 µM ABA. (*E*) Expression of HD-ZIPIII mRNAs in *phb-1d* relative to *Ler* background. *p≤ 0.05; ** p≤ 0.005; *** p ≤ 0.0005. Student's t-tests, two-tail distribution, unequal variance. Error bars, SE.

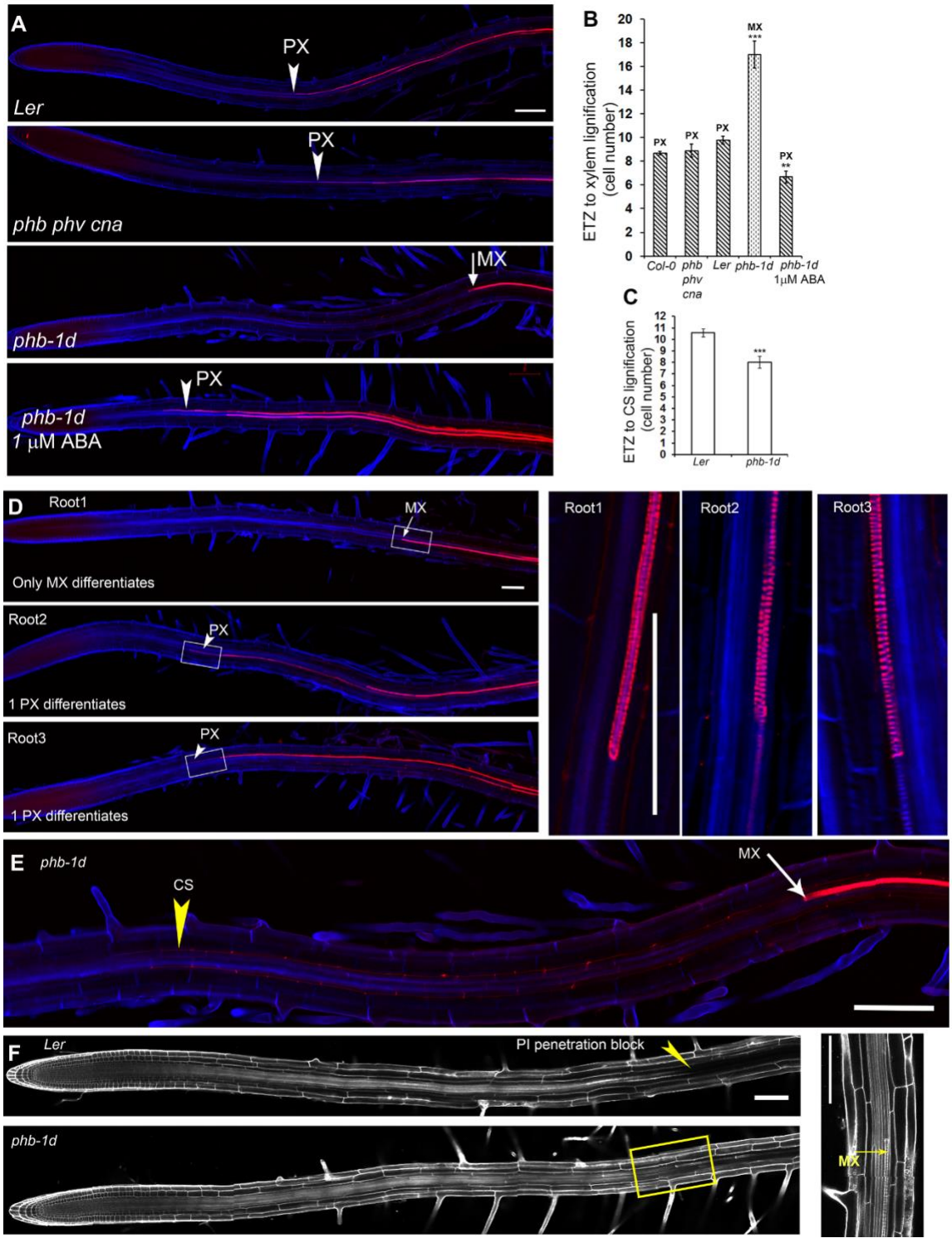

Fig. S15. **Phenotypes of *phb-1d* mutant.** (*A*) Cleared roots stained with calcofluor white (blue) for cellulosic cell wall and basic-fuchsin (red) for lignin. *Ler*, *phb;phv;can*, and *phb-1d* roots were imaged after growth in control conditions and *phb-1d* after 24-h treatment with 1 μM ABA. Positions of PX (arrowheads) and MX (arrow) lignification are indicated.

(*B*) Distance in cell number from ETZ to lignified SCW (PX or MX) (*Col-0* n=13*; phb;phv;cna* n=17; *Ler* n=16; *phb-1d* n=13; *phb-1d* treated with 1 µM ABA n=10). Statistical significance was calculated relative to *Ler*. (*C*) Distance in cell number from ETZ to Casparian strip lignification (*Ler* n=16; *phb-1d* n=13). (*D* and *E*) Cleared roots of *phb-1d* seedlings stained with calcofluor white (blue) and basic-fuchsin (red). (*D*) Root 1 is a representative image of xylem phenotype (13/15 roots) with no PX development and MX differentiation that starts in mature region of the root (17 cells from ETZ). Root 2 and Root 3 are representative of less frequent phenotypes (2/15) in which only one PX file develops and lignification starts 9 (Root 2) or 8 (Root 3) cells from the ETZ. Rectangles mark positions of enlarged areas shown at the right. (*E*) Frequent *phb-1d* phenotype depleted of PX differentiation but with normal differentiation of the Casparian strip (CS, yellow arrowhead). (*F*) *Ler* and *phb-1d* roots stained with PI (white). Yellow arrowhead indicates block of PI penetration into the stele due to penetration barrier formed by Casparian strip. Yellow rectangle in *phb-1d* marks region enlarged at the right where PI penetrates into the stele and stains MX (yellow arrow). Scale bars, 100 µm.

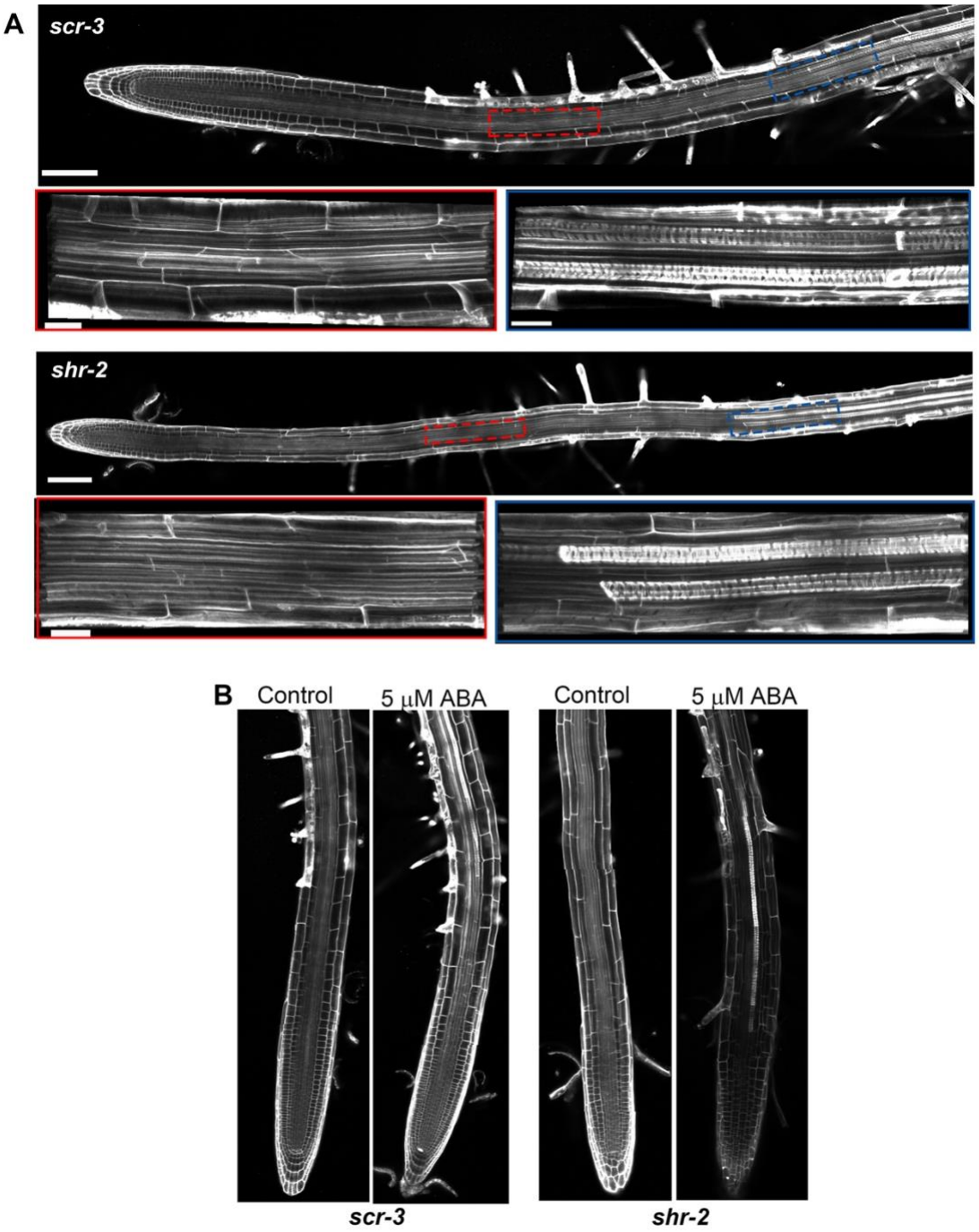

Fig. S16. **ABA treatments rescue PX specification in *shr2* and *scr3* mutants.** *(A) shr-2* and *scr-3* primary roots stained with PI (white). Red and blue dotted rectangles mark relevant enlarged regions. Note that in both mutants no PX differentiation was detected and MX differentiates later during development. *(B)* Effect of 24-h ABA treatments on PX differentiation. Note that ABA induced PX differentiation in both mutants. Scale bars in panels *A* 100 µm and 20 µm in enlarged regions, and in B 100 µm.

Table S1. Oligonucleotide primers used for quantitative RT-PCR (Q-PCR)

Gene accession	Primer name	Primer sequence 5`-3`
At3G11410	PP2C-For	TGGGATGGAGCTAGGGTTCT
	PP2C-Rev	CATACGGTTTCAAGTAATTATCACCA
At2G38310	PYL4-For	CGATCCGTAACGACCCTTC
	PYL4-Rev	CGACGTAAGACTCGACAACG
At2G34710	PHB-For	TTGGTTTCAGAACCGCAGA
	PHB-Rev	CTGTTTGAAGACGAGCAGCTT
At1G30490	PHV-For	TTGGTTCCAGAATCGCAGA
	PHV-Rev	CACTGTCTGAAGACGAGCTGA
At5g60690	REV-For	CGAGCTTGTTTATATGCAGACG
	REV-Rev	GCCAGATAGCGACCTCTCAC
At4G32880	ATHB8-For	CTCAAGAGATTTCACAACCTAACG
	ATHB8-Rev	TCACTGCTTCGTTGAATCCTT
At1G52150	ATHB15-For	CCGTCAACATACTCCAAATCC
	ATHB15-Rev	GTCACCACCGATTCACAGC
At1G70560	TAA1-For	GCCGCTCCTTTTTACTCCA
	TAA1-Rev	TGTACATACCCGACCGAACA
At1G04610	YUCCA3-For	ATCCGGTGGAAGGTACCAA
	YUCCA3-Rev	CCATACCGGAGTTTCCACAT
At5G43890	YUCCA5-For	AATCTCCATGATGTTGATGAAGTG
	YUCCA5-Rev	TCAGCCATGCAAGAATCAGT
At1G04180	YUCCA9-For	GGGCTATGGAGGGTTAGAACA
	YUCCA9-Rev	ACCAACCACCGGCAAATA
At1G13320	PP2A-For	TAACGTGGCCAAAATGATGC
	PP2A-Rev	GTTCTCCACAACCGCTTGGT

Table S2. Resources

Chemicals		
Murashige & Skoog (0.5X MS) salt mixture	Sigma-Aldrich	#M5519
+(-)cis, trans-abscisic acid (ABA)	Duchefa Biochemie	#A0941
α-naphthaleneacetic acid (NAA)	Sigma-Aldrich	#N-0640
auxinole	Ken-ichiro Hayashi, Okayama University of Science, Okayama, Japan	(Hayashi et al., 2008)
naphtylphtalamic acid (NPA)	Duchefa Biochemie	#132-66-1
poly(ethylene glycol, mol wt 8,000) PEG 8000	Sigma-Aldrich	#P5413
propidium iodide (PI)	Sigma-Aldrich	#P4864
Basic-Fuchsin	Fluka	#47860
calcofluor white	Sigma-Aldrich	#18909
Commercial Assays		
miRNeasy Micro Kit	Qiagen	217084
DNase	Qiagen	79254
High Capacity cDNA Reverse Transcription Kit	Applied Biosystems	4368814
Fast SYBR Green Master Mix	Applied Biosystems	4385612
***Arabidopsis* lines used in this study**		
Arabidopsis thaliana ecotype *Col-0*	ABRC	CS22625
Arabidopsis thaliana ecotype *Ler*	ABRC	
Arabidopsis thaliana ecotype *C24*	J. Dinneny	(26)
Col-0 35S::PYR1^{MANDI}	S. Cutler	(Park et al., 2015)
Col-0 abi1-1	ABRC	(Leung et al., 1994)
Col-0 pyr1;pyl1;pyl2;pyl4	S. Cutler	(Park et al., 2009)
Col-0 aba2-1	ABRC	(Gonzalez-Guzman et al., 2002)
Col-0 tir1-1;afb2-3;afb4-8;afb5-5	NASC	(Prigge et al., 2016)

Col-0 (er2) phb-13 phv-11 cna-2	ABRC	CS68977 (Prigge et al., 2005)
Col-0 scr-3	NASC	N3997 (Fukaki et al., 1998),
Col-0 shr-2	NASC	N2972 (Helariutta et al., 2000)
Ler phb-1d	J. Bowman	(McConnell et al., 2001)
Col-0 35S::Iaa6m1m2	E. Shani	(Li et al., 2011)
Col-0 pSCR::abi1-1	J. Dinneny	(26)
Col-0 pUAS::abi1-1	J. Dinneny	(26)
Col-0 pS18:ER-GFP	ABRC	(Lee et al., 2006)
Col-0 pVND7:GFP-NLS	T. Demura	(Kubo et al., 2005)
Col-0 pAHP6::GFP-ER	ABRC	(Bishopp et al., 2011)
Col-0 pMIR165a::GFP/pMIR166b::GFP	A. Carlsbecker	(Carlsbecker et al., 2010)
pPHB::GFP-ER	A. Carlsbecker	(Carlsbecker et al., 2010)
Col-0 pPHB:PHB-GFP	K. Nakajima	(Miyashima et al., 2011)
Col-0 DR5::Venus-NLS	M. Heisler	(Heisler et al., 2005)
Col-0 zll/pZLL::YFP:ZLL	T. Laux	(Tucker et al., 2008)
Col-0 DII-Venus	ABRC	(Brunoud et al., 2012)
C24 enhancer trap lines: J3411; J0951; J0571; Q2500; Q0990	J. Dinneny	(26)
Software		
Cell-O-Tape, CPIB macro-tool for Fiji (ImageJ)	(French et al., 2012)	
Fiji (Image J)		
Photoshop	Adobe	
ZEN	Zeiss	

References

Band, L. R., Wells, D. M., Larrieu, A., Sun, J., Middleton, A. M., French, A. P., Brunoud, G., Sato, E. M., Wilson, M. H., Peret, B., et al. (2012). Root gravitropism is regulated by a transient lateral auxin gradient controlled by a tipping-point mechanism. *Proc Natl Acad Sci U S A* **109**, 4668-4673.

Bishopp, A., Help, H., El-Showk, S., Weijers, D., Scheres, B., Friml, J., Benkova, E., Mahonen, A. P. and Helariutta, Y. (2011). A mutually inhibitory interaction between auxin and cytokinin specifies vascular pattern in roots. *Curr. Biol.* **21**, 917-926.

Brunoud, G., Wells, D. M., Oliva, M., Larrieu, A., Mirabet, V., Burrow, A. H., Beeckman, T., Kepinski, S., Traas, J., Bennett, M. J., et al. (2012). A novel sensor to map auxin response and distribution at high spatio-temporal resolution. *Nature* **482**, 103-106.

Carlsbecker, A., Lee, J. Y., Roberts, C. J., Dettmer, J., Lehesranta, S., Zhou, J., Lindgren, O., Moreno-Risueno, M. A., Vaten, A., Thitamadee, S., et al. (2010). Cell signalling by microRNA165/6 directs gene dose-dependent root cell fate. *Nature* **465**, 316-321.

Duan, L., Dietrich, D., Ng, C. H., Chan, P. M., Bhalerao, R., Bennett, M. J. and Dinneny, J. R. (2013). Endodermal ABA signaling promotes lateral root quiescence during salt stress in Arabidopsis seedlings. *Plant Cell* **25**, 324-341.

French, A. P., Wilson, M. H., Kenobi, K., Dietrich, D., Voss, U., Ubeda-Tomas, S., Pridmore, T. P. and Wells, D. M. (2012). Identifying biological landmarks using a novel cell measuring image analysis tool: Cell-o-Tape. *Plant Methods* **8**, 7.

Fukaki, H., Wysocka-Diller, J., Kato, T., Fujisawa, H., Benfey, P. N. and Tasaka, M. (1998). Genetic evidence that the endodermis is essential for shoot gravitropism in Arabidopsis thaliana. *Plant J* **14**, 425-430.

Gonzalez-Guzman, M., Apostolova, N., Belles, J. M., Barrero, J. M., Piqueras, P., Ponce, M. R., Micol, J. L., Serrano, R. and Rodriguez, P. L. (2002). The short-chain alcohol dehydrogenase ABA2 catalyzes the conversion of xanthoxin to abscisic aldehyde. *Plant Cell* **14**, 1833-1846.

Hayashi, K., Tan, X., Zheng, N., Hatate, T., Kimura, Y., Kepinski, S. and Nozaki, H. (2008). Small-molecule agonists and antagonists of F-box protein-substrate interactions in auxin perception and signaling. *Proc. Natl. Acad. Sci. USA* **105**, 5632-5637.

Heisler, M. G., Ohno, C., Das, P., Sieber, P., Reddy, G. V., Long, J. A. and Meyerowitz, E. M. (2005). Patterns of auxin transport and gene expression during primordium development revealed by live imaging of the Arabidopsis inflorescence meristem. *Curr Biol* **15**, 1899-1911.

Helariutta, Y., Fukaki, H., Wysocka-Diller, J., Nakajima, K., Jung, J., Sena, G., Hauser, M. T. and Benfey, P. N. (2000). The SHORT-ROOT gene controls radial patterning of the Arabidopsis root through radial signaling. *Cell* **101**, 555-567.

Kubo, M., Udagawa, M., Nishikubo, N., Horiguchi, G., Yamaguchi, M., Ito, J., Mimura, T., Fukuda, H. and Demura, T. (2005). Transcription switches for protoxylem and metaxylem vessel formation. *Genes Dev* **19**, 1855-1860.

Lee, J. Y., Colinas, J., Wang, J. Y., Mace, D., Ohler, U. and Benfey, P. N. (2006). Transcriptional and posttranscriptional regulation of transcription factor expression in Arabidopsis roots. *Proc Natl Acad Sci U S A* **103**, 6055-6060.

Leung, J., Bouvier-Durand, M., Morris, P. C., Guerrier, D., Chefdor, F. and Giraudat, J. (1994). Arabidopsis ABA response gene ABI1: features of a calcium-modulated protein phosphatase. *Science* **264**, 1448-1452.

Li, H., Tiwari, S. B., Hagen, G. and Guilfoyle, T. J. (2011). Identical amino acid substitutions in the repression domain of auxin/indole-3-acetic acid proteins have contrasting effects on auxin signaling. *Plant Physiol* **155**, 1252-1263.

McConnell, J. R., Emery, J., Eshed, Y., Bao, N., Bowman, J. and Barton, M. K. (2001). Role of PHABULOSA and PHAVOLUTA in determining radial patterning in shoots. *Nature* **411**, 709-713.

Miyashima, S., Koi, S., Hashimoto, T. and Nakajima, K. (2011). Non-cell-autonomous microRNA165 acts in a dose-dependent manner to regulate multiple differentiation status in the Arabidopsis root. *Development* **138**, 2303-2313.

Park, S. Y., Fung, P., Nishimura, N., Jensen, D. R., Fujii, H., Zhao, Y., Lumba, S., Santiago, J., Rodrigues, A., Chow, T. F., et al. (2009). Abscisic acid inhibits type 2C protein phosphatases via the PYR/PYL family of START proteins. *Science* **324**, 1068-1071.

Park, S. Y., Peterson, F. C., Mosquna, A., Yao, J., Volkman, B. F. and Cutler, S. R. (2015). Agrochemical control of plant water use using engineered abscisic acid receptors. *Nature* **520**, 545-548.

Prigge, M. J., Greenham, K., Zhang, Y., Santner, A., Castillejo, C., Mutka, A. M., O'Malley, R. C., Ecker, J. R., Kunkel, B. N. and Estelle, M. (2016). The Arabidopsis Auxin Receptor F-Box Proteins AFB4 and AFB5 Are Required for Response to the Synthetic Auxin Picloram. *G3 (Bethesda)* **6**, 1383-1390.

Prigge, M. J., Otsuga, D., Alonso, J. M., Ecker, J. R., Drews, G. N. and Clark, S. E. (2005). Class III homeodomain-leucine zipper gene family members have overlapping, antagonistic, and distinct roles in Arabidopsis development. *Plant Cell* **17**, 61-76.

Tucker, M. R., Hinze, A., Tucker, E. J., Takada, S., Jurgens, G. and Laux, T. (2008). Vascular signalling mediated by ZWILLE potentiates WUSCHEL function during shoot meristem stem cell development in the Arabidopsis embryo. *Development* **135**, 2839-2843.